Quaternary Science Reviews 291 (2022) 107640

Contents lists available at ScienceDirect

Quaternary Science Reviews

journal homepage: www.elsevier.com/locate/quascirev

Earthquake-triggered submarine landslides in the St. Lawrence Estuary (Québec, Canada) during the last two millennia and the record of the major 1663 CE M ≥7 event

Méril Mérindol [a, b, *], Guillaume St-Onge [a], Nabil Sultan [b], Patrick Lajeunesse [c], Sébastien Garziglia [b]

[a] Institut des sciences de la mer de Rimouski (ISMER), Canada Research Chair in Marine Geology, Université du Québec à Rimouski and GEOTOP, Canada
[b] Geo-Ocean UMR6538, Ifremer, CNRS, UBO, UBS, F-29280, Plouzané, France
[c] Département de géographie, Université Laval, Québec, Canada

ARTICLE INFO

Article history:
Received 17 February 2022
Received in revised form
28 June 2022
Accepted 1 July 2022
Available online xxx

Handling editor: A. Voelker

Keywords:
1663 CE earthquake
Canada
Geohazards
Geophysics
Holocene
Quebec
Paleoseismicity
Sedimentology
Submarine landslides
Turbidites

ABSTRACT

In eastern Canada, the Charlevoix-Kamouraska/Bas-Saint-Laurent (CKBSL) seismic zone presents a seismic hazard almost as high as that of the active Pacific zone. The major event of February 5, 1663 CE, with an estimated magnitude of ≥7, highlights the importance of this seismic hazard. The numerous submarine landslides mapped in the St. Lawrence Estuary in the CKBSL seismic zone suggest that earthquakes triggered series of submarine slope failures. In this context, the SLIDE-2020 expedition on board the RV Coriolis II in the St. Lawrence Estuary aimed to map, image and sample more than 12 zones of submarine instabilities and their associated deposits. The analysis of sediment cores sampled in the distal sedimentary deposits from these landslides reveals the presence of rapidly deposited layers (turbidites, hyperpycnites and debrites) directly linked to the submarine landslides. Dating these landslides with ^{210}Pb and ^{14}C techniques led to the identification of four periods of synchronous submarine landslides corresponding to the strongest historical earthquakes: 1663 CE, 1860/1870 CE, 1925 CE and 1988 CE (M ≥ 7, M = 6.1/6.6, M = 6.2, M = 5.9). This synchronicity over a distance reaching 220 km of several landslides supports a relationship between their triggering in the St. Lawrence Estuary and regional seismicity. The fact that as many as nine submarine landslides appear to have been triggered by the 1663 CE earthquake suggests that this event is the strongest recorded in the last two millennia in the region.

1. Introduction

One of the strongest historical earthquakes felt in eastern North America occurred on February 5, 1663, along the St. Lawrence River, in southern Québec, Canada, when the region was sparsely inhabited and the European settling was at its beginning. Therefore, the precise epicenter and magnitude of this event are estimated only from written and personal accounts of the event (Gouin, 2001). Previous studies converge to indicate that its epicenter was located in the Charlevoix-Kamouraska seismic zone (CKSZ), in the western part of the St. Lawrence Estuary (Fig. 1), although its exact localisation is still debated (Hodgson, 1928; Locat, 2011; Locat *et al.*, 2003; Locat et al., 2016; Pinet et al., 2021). Gouin (2001) has compiled testimonies of damage to barns, chimneys and houses in eastern America in an area reaching 600 km around the suspected epicenter. From this historical data, Ebel (2011) estimated the magnitude (M) of the 1663 earthquake at 7.5 while the Canadian catalog of historical earthquakes, used to map the seismic hazard in Canada, considers a magnitude slightly lower, of M = 7 (Smith, 1962; Lamontagne et al., 2018).

Jesuits writings contemporary to the 1663 CE earthquake (e.g., Ebel, 1996) report "the formation of new lakes", "the disappearance of mountains" and "the displacement of forest down to the St. Lawrence River" as consequences of subaerial landslides most likely triggered by the 1663 earthquake. The historical observations are consistent with studies carried out on regional landslides which established a link between the 1663 CE earthquake and the

* Corresponding author. Geo-Ocean UMR6538, Ifremer, CNRS, UBO, UBS, F-29280, Plouzané, France.
E-mail address: meril.merindol@ifremer.fr (M. Mérindol).

https://doi.org/10.1016/j.quascirev.2022.107640
0277-3791/

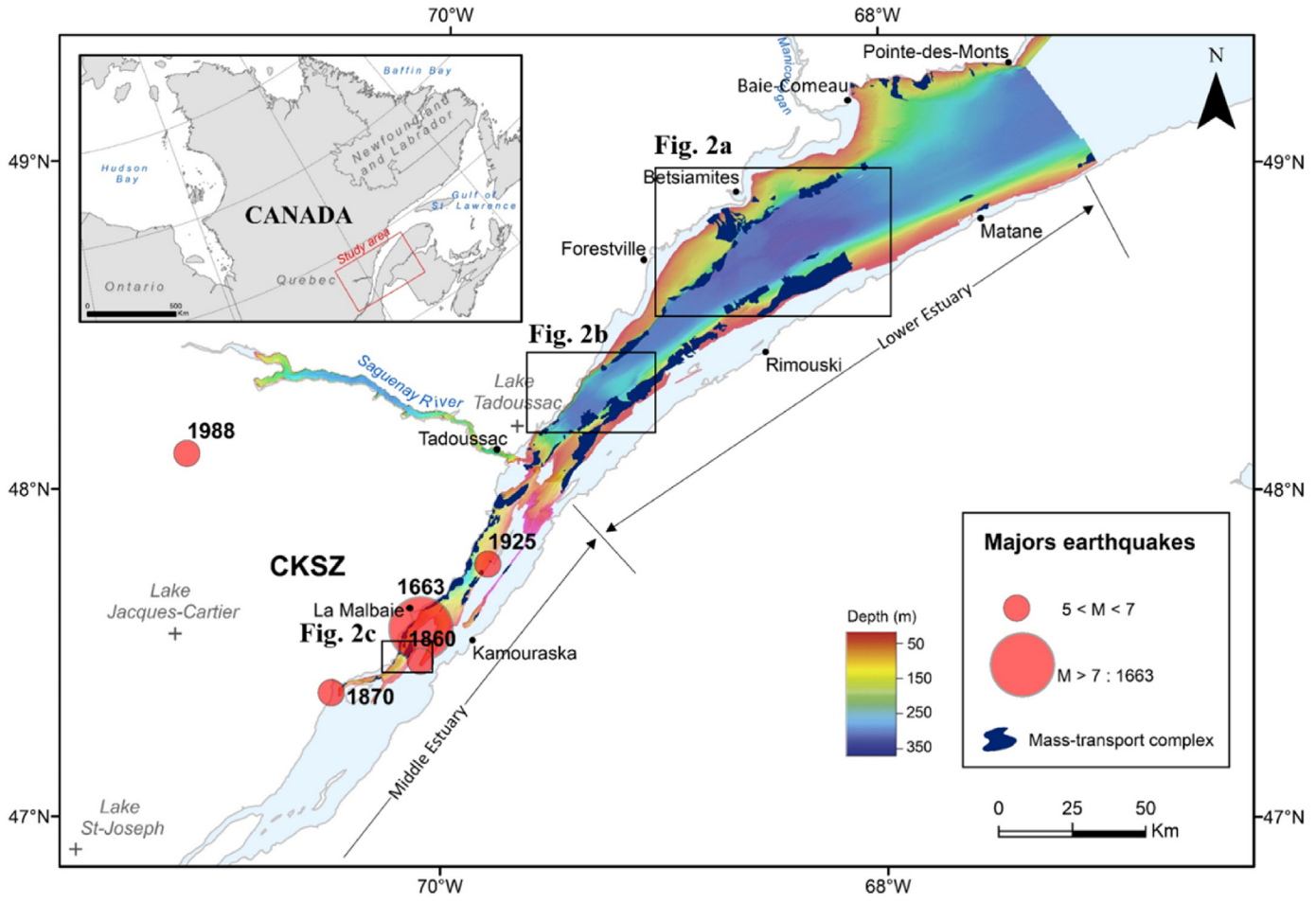

Fig. 1. Bathymetric map of the St-Lawrence Estuary and location of significant East Canadian Earthquakes of the period 1663-2005 (red circles) from Lamontagne et al. (2018). Dark blue areas indicate the mass-transport complexes mapped by Pinet et al. (2015). CKSZ corresponds of the Charlevoix-Kamouraska Seismic Zone. (For interpretation of the references to color in this figure legend, the reader is referred to the Web version of this article.)

landslides observed at Saint-Jean-Vianney (Lasalle and Chagnon, 1968), the Gouffre River (Filion et al., 1991), the Mont-Eboulé (Dubé, 1998) and Colombier (Cauchon-Voyer et al., 2008). The recent study conducted in the CKSZ (Fig. 1) by Pinet et al. (2015), indicates that more than one hundred submarine mass-movements occurred in the St. Lawrence Estuary. The high density of submarine landslides in the CKSZ suggests a possible link between submarine slope destabilization and seismicity (e.g., Cauchon-Voyer et al., 2008). Some submarine landslides have been related to regional seismicity such as in the Betsiamites River area, where Cauchon-Voyer et al. (2008), (2011) combined terrestrial and marine data to relate submarine landslides to major earthquakes occurring before 9280 cal yr BP, in 7250 cal yr BP and in 1663 CE. Other authors have observed this relationship in Québec using geomorphological, sedimentological and dating methods but outside the St. Lawrence Estuary such as in the Saguenay Fjord (Syvitski and Schafer, 1996a; 1996b; Locat et al., 2003; St-Onge et al., 2004) and in lacustrine environments (Doig, 1990; Ouellet, 1997; Locat et al., 2016; Trottier et al., 2019).

Submarine landslides, through erosion of the seafloor and incorporation of sediments and water, can evolve into a debris flow and a turbidity current (Bryn et al., 2005; Strachan, 2008). Over the last two decades, the marine turbidite record has been increasingly used as a proxy for earthquake recurrence (Lebreiro et al., 1997; Gracia et al., 2010; Goldfinger et al., 2012; St-Onge et al., 2012; Ratzov et al., 2015; Piper et al., 2019; Howarth et al., 2021). The recurrence of strong regional earthquakes and the risks they pose when associated with submarine slope failures can have major impacts on coastal environments (e.g., damage to coastal infrastructures and threats to coastal communities, risk of tsunamis, cable rupture, coastal erosion), particularly with increasing human populations along the coast. It is therefore essential to improve our knowledge of natural hazards by establishing a chronology of submarine landslides triggered by earthquakes.

Mapping and dating of submarine landslides at a regional scale provide the opportunity to assess their synchronicity and thus their possible triggering by an earthquake (Goldfinger et al., 2012, 2017; Patton et al., 2015). This paper involves 19 sediment cores recovered near 12 submarine landslides located over a distance of ~220 km in the St. Lawrence Estuary with the aim of: (1) identifying and characterizing rapidly deposited layers (RDLs) resulting from landslides (e.g., debrite, turbidite) dated by radiocarbon and ^{210}Pb; and (2) relate them to historical earthquakes (Fig. 1).

2. Regional setting

2.1. The St. Lawrence Estuary (Eastern Canada)

The St. Lawrence Estuary, located in Québec (eastern Canada), is one of the world's largest estuarine basins (~8000 km^2). It is

generally considered to be divided into two parts: the Lower Estuary, from the mouth of the Saguenay River to Pointe-des-Monts, and the Middle Estuary, upstream and southwest of the Saguenay River (Fig. 1) (e.g., Pinet et al., 2011). The maximum water depth of 355 m is reached in the central part of the estuary, in the Laurentian Channel, where the seafloor presents a sub-horizontal depression ~900 km long. This major feature is a U-shaped incised-valley bounded by steep escarpments inherited from Quaternary glacial successive erosions (Josenhans and Lehman, 1999; Shaw et al., 2002) and phases of preglacial subaerial erosion (King and MacLean, 1970). In the Lower Estuary, its topography is mostly shaped by mass-transport deposits and pockmarks (Locat et al., 2003; Pinet et al., 2008). In this study, six regions with submarine landslides were considered representing the estuary over its entire length (Fig. 1 and Table 1). The Rimouski, Baie-Comeau and Betsiamites sectors are located in the eastern part of the Lower Estuary and the Forestville and Saguenay sectors are located in its western part. Only the La Malbaie area is located in the Middle Estuary.

The basement of the St. Lawrence Estuary is mostly composed of carbonate and siliciclastic rocks from the St. Lawrence Platform (Duchesne et al., 2007). It is predominantly covered by Quaternary sediments, except in narrow strips at Anticosti and Mingan (Haworth, 1978). The St. Lawrence Platform is bordered to the north by the Grenville Formation, composed of metamorphic rocks, and to the south by the Appalachian Mountains, composed of Paleozoic sedimentary rocks (e.g., Duchesne et al., 2007). Less resistant to erosion, the Laurentian Channel is parallel to these two formations (Pinet et al., 2008). The estuary is divided into three physiographic regions: the shelf, the slope and the Laurentian Channel. In the Middle Estuary, the shelf is reduced and even absent (Figs. 1 and 2).

Inputs of sediments to the estuary originate from five main rivers in addition to the St. Lawrence River: the Saguenay, Rimouski, Betsiamites, Aux-Outardes and Manicouagan Rivers. The associated discharge areas correspond to gently sloping submarine fans (Pinet et al., 2015) with active turbiditic channels (Normandeau et al., 2017). One of the largest mass-transport complexes is located near a former mouth of the Betsiamites River (Cauchon-Voyer et al., 2008). Holocene mass-transport deposits are not consistently present near the mouth of major rivers, suggesting that the actual sedimentary inputs are not the predominant preconditioning factor for seafloor instability (Normandeau et al., 2015). However, most of them are located on steep slopes (>5°) bordering the Laurentian Channel, indicating that the seafloor gradient is an important preconditioning factor for slope instability (Normandeau et al., 2015; Pinet et al., 2015). If gas charging is considered a preconditioning factor for submarine slope instability (e.g., Riboulot et al., 2013), no link was clearly established between the presence of free gas and the mass-transport complexes in the St. Lawrence Estuary (Pinet et al., 2015).

Table 1
Location and length of the studied cores.

Area and core name	Zone	Lat. (°N)	Long. (°W)	Length (m)
Rimouski				
COR20-02-03 GC	Slope	48°34.71	68°29.66	3.87
Baie-Comeau				
COR20-02-13 GC	Slope - Deposit	48°58.71	68°10.74	4.20
COR20-02-14 GC	Deposit	48°57.94	68°12.25	3.87
Betsiamites				
COR20-02-17 GC	Deposit	48°53.27	68°29.93	3.45
COR20-02-18GC/BC	Deposit	48°50.97	68°32.10	3.97
COR20-02-04 GC	Lobe	48°34.77	68°29.76	3.86
COR07-03-11 PC	Deposit	48°48.58	68°38.34	2.45
COR07-03-13 PC	Scar	48°51.10	−68°37.24	4.09
COR20-02-19 GC	Deposit	48°48.37	68°37.30	2.32
Forestville				
COR20-02-20GC/BC	Deposit	48°27.96	69°10.04	5.05
COR20-02-21 GC	Deposit	48°21.14	69°08.47	2.49
Saguenay				
COR20-02-26GC/BC	Deposit	48°12.25	69°31.87	2.83
COR20-02-28GC/BC	Deposit	48°12.88	69°25.87	1.01
COR20-02-29 GC	Deposit	48°11.82	69°27.40	1.60
La Malbaie				
COR20-02-50 GC	Deposit	47°30.72	70°10.84	2.28

2.2. Quaternary sedimentation

The carbonate platform of the St. Lawrence Estuary is covered by Quaternary sediments with a maximum thickness of ~400 m controlled by the underlying topography of the bedrock (Duchesne et al., 2010). The seismo-stratigraphic sequence of Quaternary sedimentation in the St. Lawrence Estuary, first established by Syvitski and Praeg (1989), and completed with samples and dating (St-Onge et al., 2008; Duchesne et al., 2010), is composed of five units. Seismic Unit 1 overlies the bedrock. It is interpreted as ice-contact sediments (Syvitski and Praeg, 1989) when the ice extension was maximum during the Last Glacial Maximum (LGM: 21,000 cal yr BP). Unit 2 corresponds to ice-proximal, coarse-grained sediments in a glaciomarine environment. Fine-grained, ice-distal sediments characterize Unit 3. Units 2-3 were deposited when the Goldthwait Sea was present in the St. Lawrence Estuary and Gulf from 13,000 to 9000 cal yr BP (Dionne, 2001). Unit 4 marks the transition between glaciomarine and postglacial sedimentation. It comprises hemipelagic sediments (Duchesne et al., 2010) following the rerouting of meltwaters of the Laurentide Ice Sheet (LIS) from the St. Lawrence to Hudson Bay after the collapse of the proglacial Lake Agassiz-Ojibway around 8500 cal yr BP (St-Onge et al., 2003). Cauchon-Voyer et al. (2011) described stratified silty clays with thin layers of sand in Unit 4. Finally, Unit 5 differs from Unit 4 by the presence of coarser sediments that were deposited under modern oceanographic conditions. Modern sedimentation rates range between 0.74 cm.yr^{-1} at the mouth of the Lower Estuary to 0.04 cm.yr^{-1} in the Gulf, with an exponential decrease (Zhang, 2000).

2.3. Regional seismicity and sediment liquefaction

In addition to the 1663 CE earthquake, four earthquakes with M 5.9 to 6.6 occurred in the CKSZ in 1860, 1870, 1925 and 1988 CE (Smith, 1962; Lamontagne et al., 2003; Lamontagne et al., 2018) (Fig. 1). An average of 200 earthquakes are recorded annually in CKSZ and 50 to 100 in the Lower St. Lawrence zone (Lamontagne et al., 2003). They are localized at depths between 5 and 25 km in the Precambrian bedrocks (Anglin, 1984). Only a small proportion exceeds M 3.

The origin of intraplate earthquakes in Eastern Canada is not clearly identified, but two principal causes are conceivable: tectonic and glacio-isostatic (Wu, 1998). Most earthquakes are concentrated in the St. Lawrence Valley and related to a fault inherited from Paleozoic rifting (Adams and Basham, 1989). The depth of the hypocenters corresponds to the Appalachian thrust fault over the St. Lawrence Platform, named Logan fault (Anglin, 1984). These evidences support a tectonic origin but only a portion of the recorded earthquakes can be related to tectonics.

Thus, regional studies highlighted a higher frequency of mass movements in the early Holocene (St-Onge et al., 2004; Cauchon-Voyer et al., 2011) and liquefaction events interpreted as markers of enhanced seismic activity between 8000 and 1000 cal yr BP (Obermeier et al., 1992). These observations are consistent with deglaciation in the St. Lawrence region, which resulted in significant glacio-isotactic adjustment during the early Holocene (Wu, 1998).

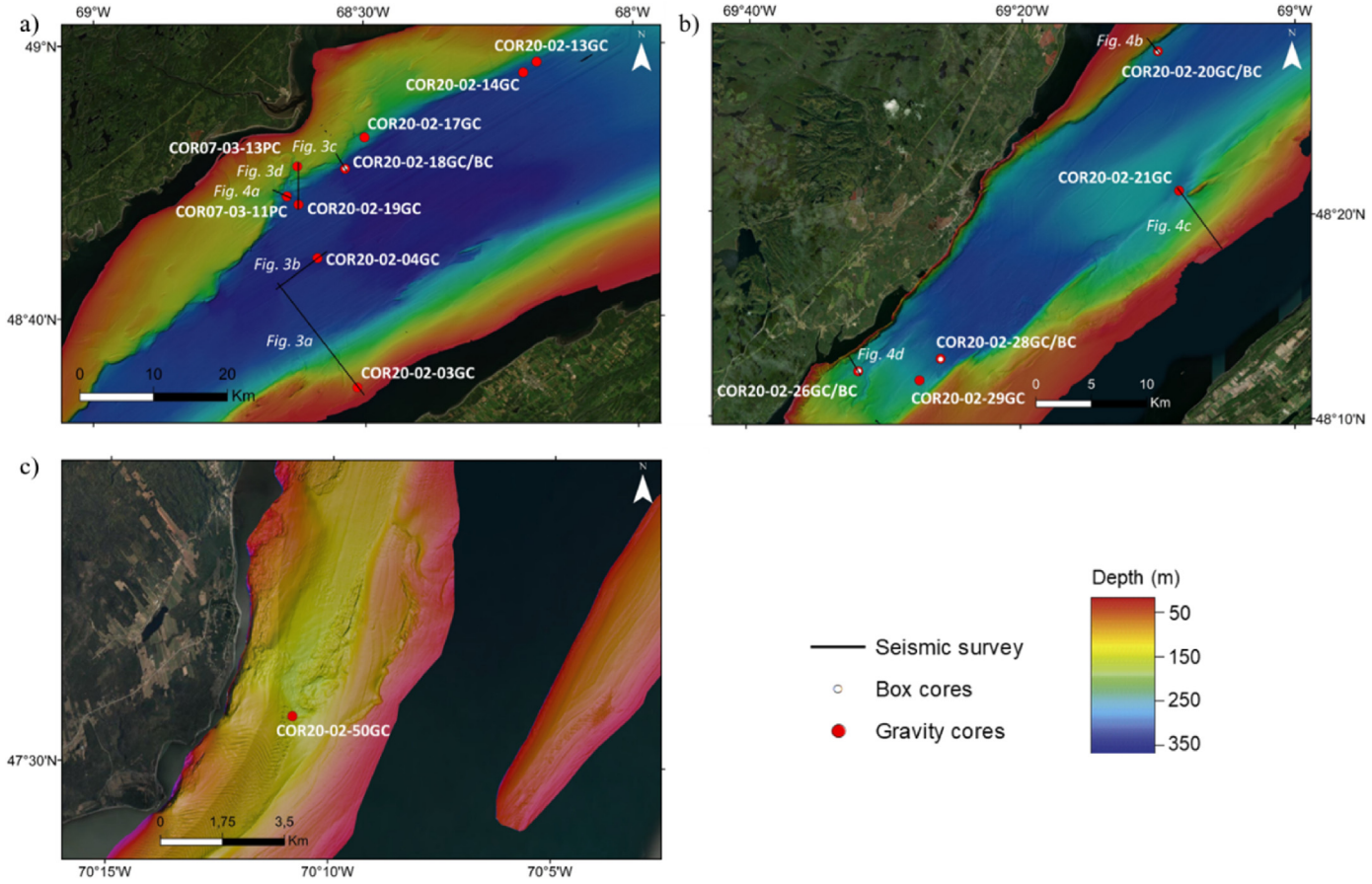

Fig. 2. Bathymetric maps of the Betsiamites – Baie Comeau – Rimouski a), of the Forestville – Saguenay b) and of the Charlevoix sectors c). The gravity and box cores are respectively represented by red and white circles. The black lines correspond to track lines of the acoustic sub-bottom profiler survey. (For interpretation of the references to color in this figure legend, the reader is referred to the Web version of this article.)

In addition to tectonic and glacio-isostatic processes, earthquakes can be influenced by fracturing caused by an asteroid impact in the Charlevoix region about 350 Ma ago (Roy and DuBerger, 1983). The weakness of the fractured crust coupled with glacio-isostatic rebound could partially explain regional seismicity and the high earthquake concentration observed by Roy and DuBerger (1983) in the CKSZ.

Seismicity is the main cause of sediment liquefaction (Seed and Idriss, 1967) which can destabilize submarine slopes and generate submarine landslides (Tuttle and Atkinson, 2010). Indeed, Cauchon-Voyer et al. (2008, 2011) suggest that the alternation of silty clays and sand layers in Unit 4 of the St. Lawrence Quaternary sedimentation could influence the permeability of materials and favor an increase in pore pressure in the case of an earthquake. Consequently, a weak layer in Unit 4 could be generated during an earthquake, thus promoting the development of slip surface. Based on geotechnical analyses and numerical simulations, Martin et al. (2001) showed that this alternation of silty clays and sand in Saguenay Fjord sediments implies high liquefaction susceptibility during an earthquake.

3. Data and methods

3.1. Geophysics

High-resolution swath bathymetry data was collected from 1997 to 2005 between Île-aux-Coudres and Pointe-des-Monts by the Canadian Hydrographic Service using multibeam echosounder systems mounted on the Coast Guard Ship *Frederick G. Creed* (before 2005: Kongsberg EM-1000; in 2005: EM-1002) and launch *Guillemot* (before 2005: EM-3000; in 2005: EM-3002). These surveys provided a full-bottom coverage below 30 m depths at a resolution of 5 m.

In summer 2020, the bathymetric coverage was completed during the SLIDE-2020 cruise on board the RV *Coriolis II* using a Kongsberg EM-2040 multibeam echosounder system coupled with the Applanix POS/MV inertial platform. Surveys were conducted in areas where Pinet et al. (2015) had previously mapped mass-transport complexes with the aim to significantly increase the resolution. A new bathymetric grid with a cell size of 1 m was generated using the Caris Hips & Sips software. Data acquired during the SLIDE-2020 cruise with the celerimeter *Minos* from *AML oceanographic* were used to account for the variability of sound velocity in the water column.

In addition, high-resolution seismic data were collected (Figs. 3 and 4) using the hull-mounted Edgetech X-Star 2.1 subsurface profiler. Hence, about 1500 km of seismic profiles were acquired during the SLIDE-2020 expedition. The source frequency was between 2 and 12 kHz with chirp pulses between 3 and 20 ms. Time-to-depth conversion of the seismic profiles was done using an average sound wave velocity value of 1500 $m.s^{-1}$ corresponding to the velocity in water and the mean value measured on sediment cores using the Multi Sensor Core Logger. Interpretation of the seismostratigraphic sequence was based on seismic attributes such

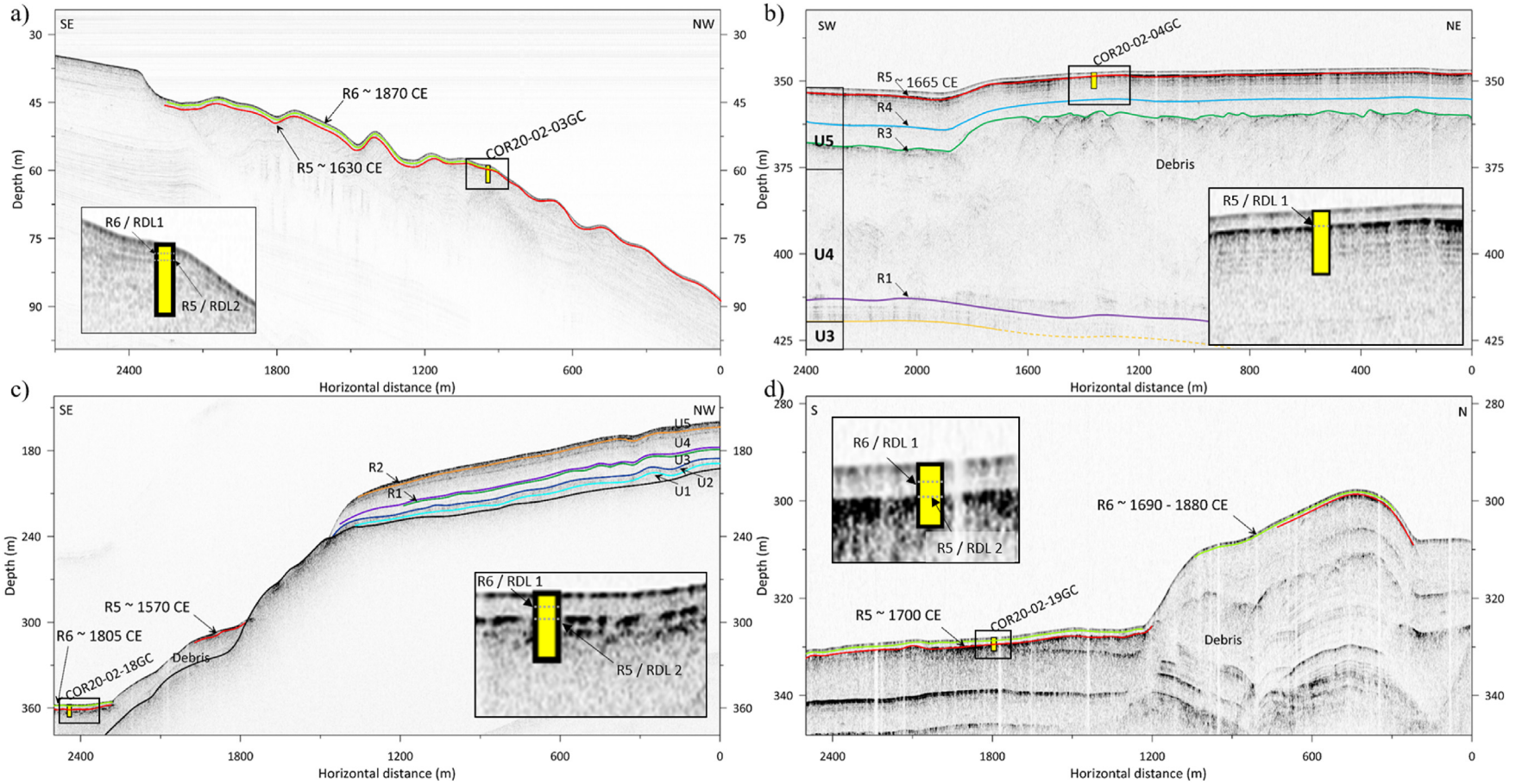

Fig. 3. a) Seismic profile RIM_1T (see Fig. 2 for the locations) on which reflectors R5 and R6 corresponds respectively to turbidites T2 and T1 in core COR20-02-03 GC. b) Seismic profile RIM_1A, transversal to the Betsiamites lobe in the Laurentian Channel. Labels U3 to U5 refer to seismic units and R1 to R5 to seismic horizons described by Cauchon-Voyer et al. (2008). The black square is a close-up view of R5. Reflector R5 correlates with turbidite T1 in the core 20-02-04 GC. c) Seismic profile BET_B_2T with R5 and R6 reflectors (cf. detailed view in the black square) which correspond to turbidites T3 and T2 in COR20-02-18 GC. d) Southern part of seismic profile BET_D_2T. Core COR20-02-19 GC reaches reflectors R6 and R5 at ~0.5 mbsf and ~1.2 mbsf, which are respectively interpreted as turbidites T1 and T2. See supplementary data for uninterpreted seismic profiles.

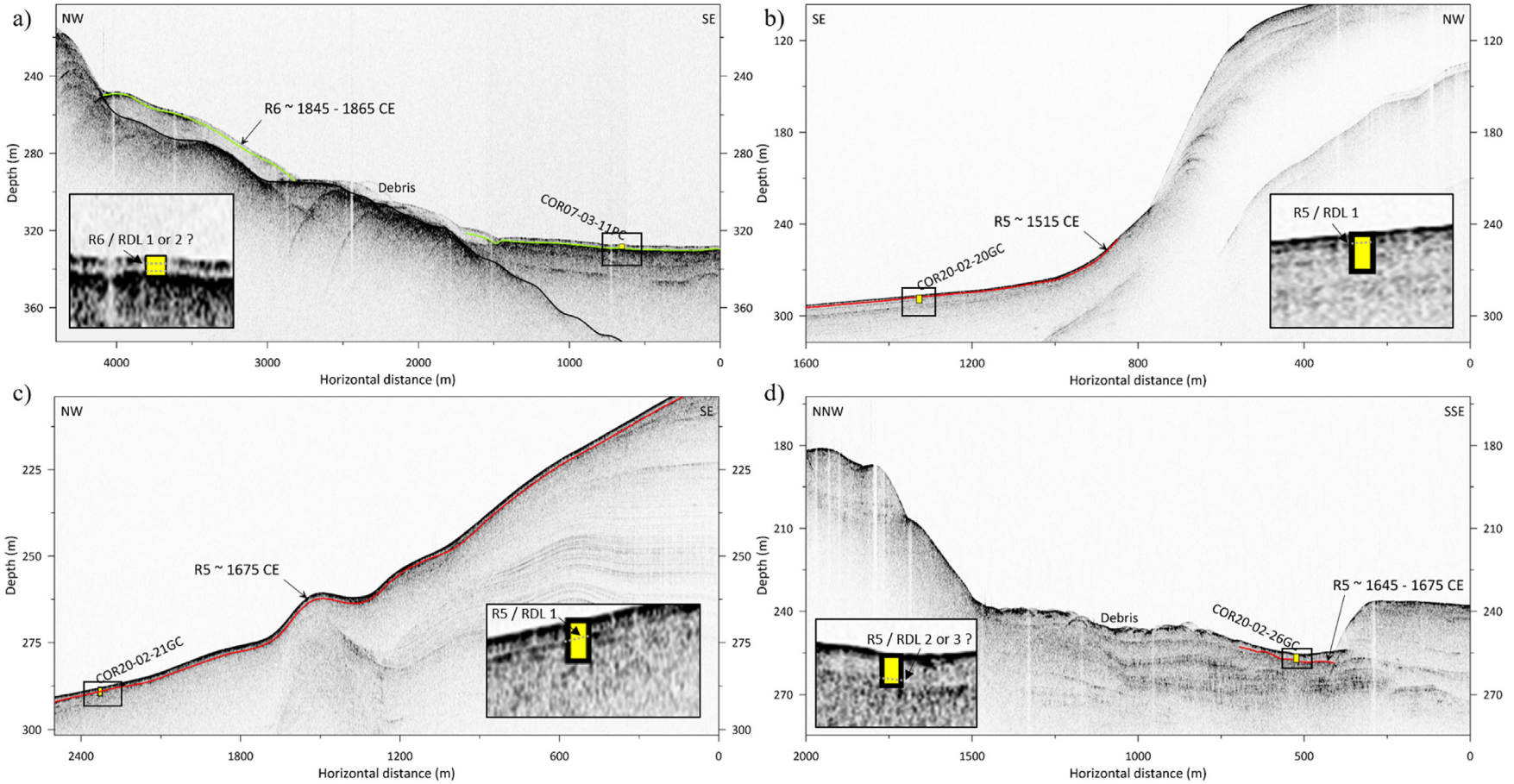

Fig. 4. a) Seismic profile BET_D_3T in the Betsiamites area (see Fig. 2 for the locations). The reflector R6 reached by core COR07-03-11 PC, corresponds to turbidite T1 or T2 dated around 1845–1865 CE. b) Seismic profile FOR_A_1T. Turbidite T1 in COR20-02-20 GC corresponds to R5. c) Seismic profile ESC_BCD_1T. Reflector R5 (cf. detailed view in the black square) correlates with turbidite T1 sampled in core COR20-02-21 GC. See supplementary data for the uninterpreted seismic profiles. d) The seismic profile SAG_H_1T with reflector R5 at the toe of a mass transport deposit. It corresponds to turbidites T2 or T3 observed in core COR20-02-26 GC. See supplementary data for the uninterpreted seismic profiles.

as reflections, geometry and amplitude of reflecting horizons detailed by Cauchon-Voyer et al. (2008).

3.2. Core sampling

During the SLIDE-2020 expedition, cores were recovered over a distance of more than 200 km along the St. Lawrence Estuary, at water depths between 34 and 354 m (Fig. 2). The cores were collected in the CKBSL seismic zone. All thirteen gravity cores and four box cores recovered during SLIDE-2020 are used in this study (Table 1 and Fig. 2). Box cores were subsampled with push cores connected to a pump to avoid compaction of sediment. Unlike gravity cores, they do not disturb the sediment/water interface, which allows for correlation of the gravity and box cores, as well as the use of ^{210}Pb dating on the box cores. The gravity corer used had a maximum length of 6 m. This study also used two piston cores of 2.5 m and 4.1 m long that were recovered during the COR07-03 expedition (RV *Coriolis II*, Cauchon-Voyer et al., 2007).

The core sites are located in the distal part of the mass-transport deposit in order to sample the finest part of the submarine landslide allowing to date the hemipelagic sediment above and below the RDLs. The targeted RDLs are theoretically not affected by local sedimentary processes because they were selected neither at the mouth of active rivers, nor at the end of active turbidity current channels (e.g., Normandeau et al., 2017), or in pockmark-rich areas described by Pinet et al. (2015). However, due to the estuarine context, regional sedimentary processes such as hyperpycnal flows could occur in the St. Lawrence Estuary.

3.3. Sedimentological analyses

Wet bulk density, low-field volumetric magnetic susceptibility (k) and P-Wave velocity were measured using the GEOTECK MSCL (Multi Sensor Core Logger) at ISMER (St-Onge et al., 2007, Figs. 5 and 6). Measurements were performed at intervals of 1 cm on whole sections of gravity cores and 0.5 cm on whole sections subsampled from the box cores.

After splitting the cores, archived halves were photographed and described (texture, color, lithology, structures and bioturbation). Subsequent digital X-ray images were then acquired with the GEOTECK XCT scanner. This non-destructive measurement allows to visualize the sedimentary structures. The denser materials that compose the RDLs appear as light gray on the X-ray images. On split cores, bulk magnetic susceptibility (k) was measured with a point source sensor, while L^*, a^* and b^* color parameters were determined using the Minolta CM-2600d spectrophotometer at 1 cm intervals (Figs. 5 and 6). Because k increases slightly with increasing grain size, this parameter is used to identify RDLs following the method presented by St-Onge et al. (2007). Grain-size analysis (1–2000 μm) was performed using the Master Sizer 3000 (Malvern) laser grain size analyzer with sampling intervals of 1–2 cm in each RDL and 5–20 cm for the background sedimentation. Prior to their analysis, the samples were diluted in a solution composed of distilled water and hexametaphosphate and stirred for 24 h to deflocculate clay particles.

The geochemical composition was measured on archive halves using the non-destructive Olympus Innov-X Delta X-Ray Fluorescence (XRF) scanner in line with the MSCL. The spacing of XRF measurements was similar to that of the other measurements previously mentioned. In this study, the Ca/Fe ratio (biogenic/detrital proxy) and the Rb/Zr ratio (grain size proxy) were used as criteria to identify RDL (Croudace et al., 2006) and to help distinguish the top of RDLs from hemipelagic sedimentation (Figs. 5 and 6). RDLs are numbered between 1 for the youngest and 7 for the oldest and are site-specific. As such, the RDL numbers do not refer to the synchronicity of the deposits.

3.4. Dating

Radiocarbon dating was performed on 45 samples of shells or organic matter that were sampled close to the bases of RDL in the hemipelagic sediments (Table 2). After pre-treatment and graphitization at the *Centre d'études nordiques* at Université Laval (Québec City), they were measured at the Keck-Carbon Cycle AMS facility at the University of California Irvine (USA). To obtain accurate RDL chronology, the ^{14}C ages of hemipelagic samples were calibrated using the Calib 8.2 software (Stuiver and Reimer, 1993) and the Marine20 curve (Heaton et al., 2020). To consider the local offset from the global ocean reservoir (ΔR), two reservoir ages from McNeely et al. (2006) were used. These reservoir ages are closest to the study area with one at Matane of $\Delta R = 77 \pm 60$ ^{14}C yr and one at Pointe John of $\Delta R = -13 \pm 70$ ^{14}C yr. They were averaged to have a final reservoir age of $\Delta R = 39 \pm 63$ ^{14}C yr for shell samples. Finally, the radiocarbon ages were converted to calendar ages (CE) for comparison with historical earthquakes (Table 2).

To construct the best-fit age models, the R software package Bacon 2.3 (Blaauw and Christen, 2011) was used. It considers Bayesian statistics with a normal distribution. Both standard deviations of 1 σ (probability of 0.95) and 2 σ (probability of 0.68) were used in calculations (Fig. 7). In these calculations, turbidite erosion was assumed negligible because it was not possible to quantify basal erosion.

Sedimentation rates were derived from ^{210}Pb measurements on sediments from 4 box cores (Table 3 and Fig. 8). The cores were sampled at intervals ranging from 1 to 5 cm and freeze-dried, then ground to a fine, homogenous powder. The ^{210}Pb activity was measured using a GMX50-S gamma counter from Ortec and GX7020 counter from Canberra. Considering the constant flux and constant rate model (Appleby and Oldfield, 1978), the sedimentation rates (cm.yr^{-1}) were derived from the slope of Ln (^{210}Pb$_{excess}$) in the region of radioactive decay (Fig. 8). The ages of turbidites were then calculated by extrapolating a constant sedimentation rate down to the hemipelagic depth of turbidites. Sediment compaction is neglected because the density curve of hemipelagic sedimentation appears constant with depth (Fig. 8).

4. Results

4.1. Facies identification

The four cores presented in Figs. 5 and 6 show the sedimentary facies observed on analyzed cores. They were selected to best illustrate the characteristics of the different types of RDLs. An exhaustive list of all the sediment cores is presented in the supplementary data. The results of core analysis identified two mains facies: hemipelagites and RDLs (Figs. 5 and 6). Hemipelagites are consistent with normal "background", hemipelagic sedimentation while RDLs are a result of almost instantaneous deposition. Hemipelagites consist of homogenous gray-colored silts (Munsell value 5 YR 5/1). The gray tone varies with the intensity of bioturbation from dark gray (5 YR 4/1) to very dark gray (5 YR 3/1). The hemipelagites are composed of 10–20% clay (<2 μm), 65–75% silt (2–63 μm) and 10–20% sand (63 μm - 2 mm). Their gamma density values are constant with depth and oscillate between 1.4 and 1.6 g cm^{-3}. On X-ray images, hemipelagites appear in homogenous black gray and their values of magnetic susceptibility are relatively low (~125.10^{-5} SI) compared to RDLs (~500.10^{-5} to 750.10^{-5} SI). Overall, hemipelagites have the same properties across the St.

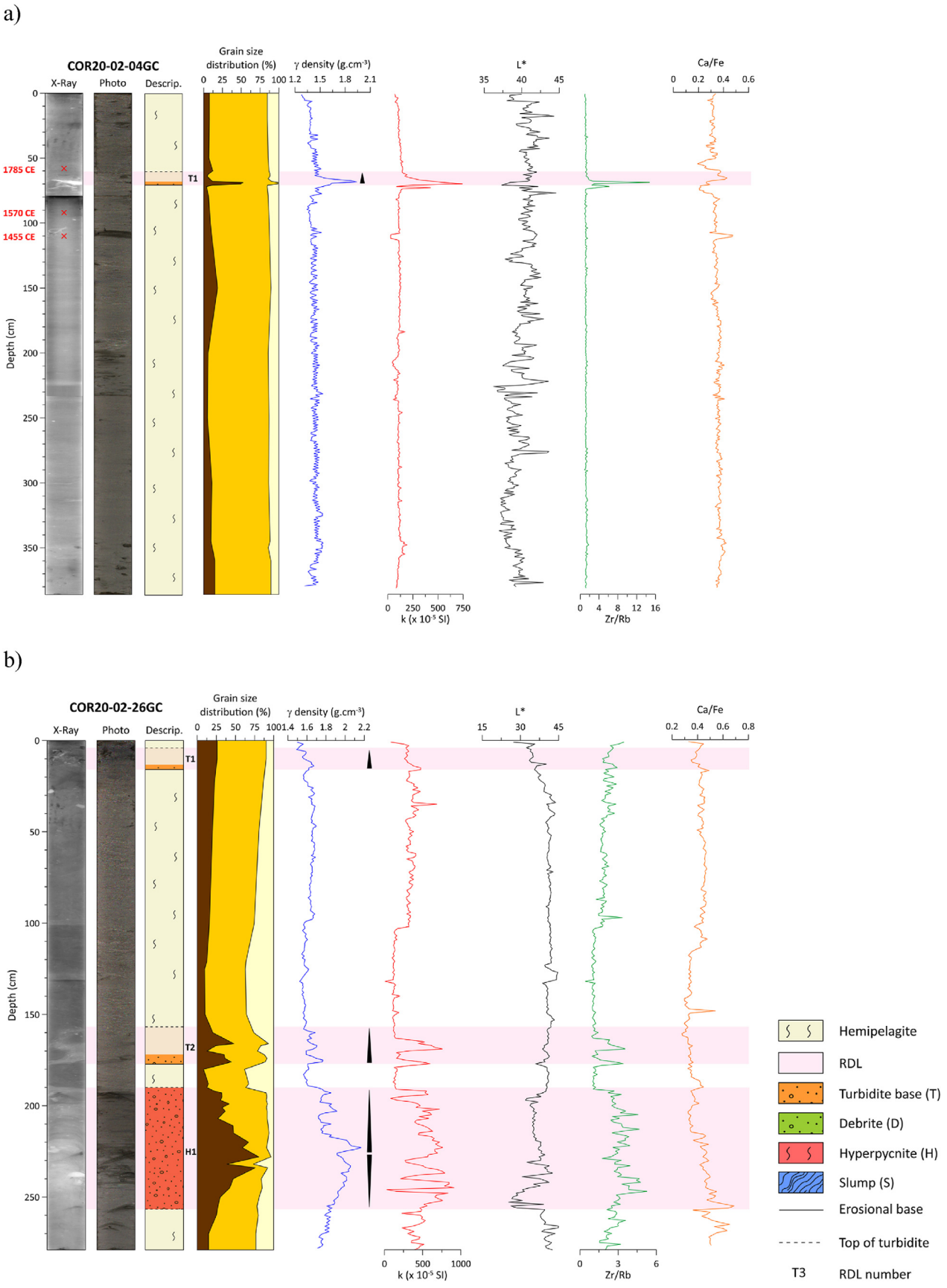

Fig. 5. Results of the sedimentological analyses carried out on cores a) COR20-02-04 GC and b) COR20-02-26 GC. From left to right: X-ray image, digital photography, sedimentological description, γ-density, magnetic susceptibility *k*, lightness *L**, Zr/Rb and Ca/Fe.

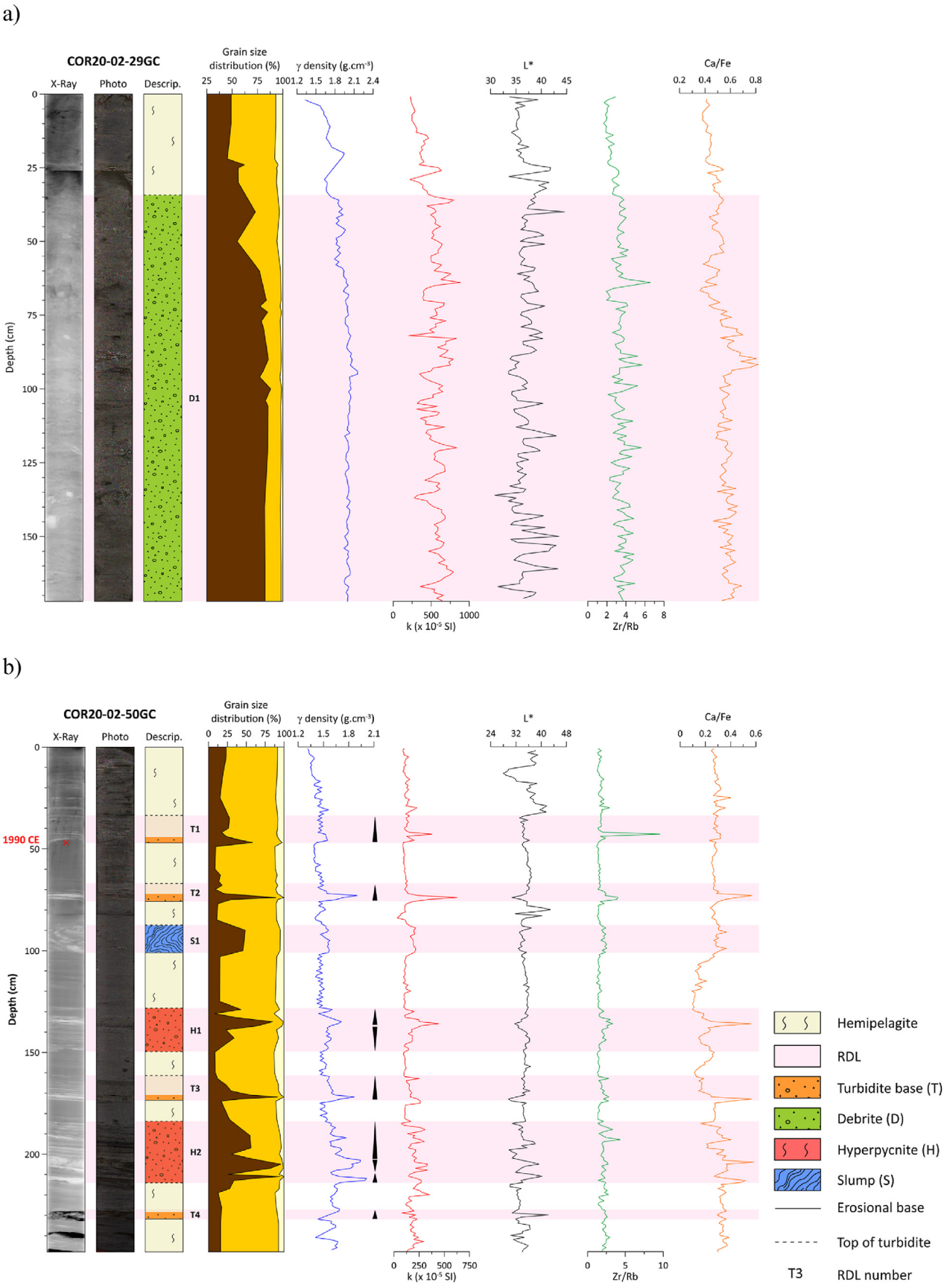

Fig. 6. Results of the sedimentological analyses carried out on cores a) COR20-02-29 GC and b) COR20-02-50 GC. From left to right: X-ray image, digital photography, sedimentological description, γ-density, magnetic susceptibility *k*, lightness *L**, Zr/Rb and Ca/Fe.

Table 2
Radiocarbon analyses from cores recovered in the St. Lawrence Estuary (Québec).

Core	Lab. num.	Depth (cm)	Sample type	^{14}C age (BP)	ΔR	Calibrated age (yr BP) ± 1σ	Calibrated age (CE) ± 1σ
COR07-03-13 PC	ULA-9628	10.00	Organic matter	255 ± 15	–	300 ± 5	1650 ± 5
COR20-02-03 GC	ULA-9787	8.00	Shell	Modern	39 ± 63	−55 ± 5	2005 ± 5
	ULA-9788	89.50	Shell	765 ± 15	39 ± 63	180 ± 95	1770 ± 95
	ULA-9789	99.50	Shell	780 ± 20	39 ± 63	195 ± 100	1755 ± 100
	ULA-9790	135.50	Shell	920 ± 15	39 ± 63	345 ± 85	1605 ± 85
	ULA-9791	356.75	Shell	2020 ± 20	39 ± 63	1380 ± 90	570 ± 90
COR20-02-04 GC	ULA-9645	47.00	Shell	745 ± 15	39 ± 63	165 ± 95	1785 ± 95
	ULA-9642	92.50	Shell	965 ± 15	39 ± 63	380 ± 80	1570 ± 80
	ULA-9644	109.50	Shell	1095 ± 15	39 ± 63	495 ± 80	1455 ± 80
COR20-02-13 GC	ULA-9652	17.50	Shell	1190 ± 15	39 ± 63	570 ± 50	1380 ± 50
	ULA-9653	19.50	Shell	1210 ± 15	39 ± 63	585 ± 70	1365 ± 70
	ULA-9647	84.75	Shell	2915 ± 15	39 ± 63	2465 ± 115	−515 ± 115
	ULA-9648	161.50	Shell	4875 ± 15	39 ± 63	4920 ± 110	−2970 ± 110
COR20-02-14 GC	ULA-9792	9.25	Shell	675 ± 20	39 ± 63	110 ± 80	1840 ± 80
	ULA-9793	46.0.	Shell	1640 ± 15	39 ± 63	995 ± 95	955 ± 95
	ULA-9794	65.00	Shell	2020 ± 15	39 ± 63	1380 ± 175	570 ± 175
	ULA-9816	71.50	Shell	2125 ± 15	39 ± 63	1490 ± 195	465 ± 195
	ULA-9817	97.50	Shell	2780 ± 15	39 ± 63	2280 ± 220	−330 ± 220
COR20-02-17 GC	ULA-9818	73.50	Shell	1655 ± 20	39 ± 63	1010 ± 95	940 ± 95
	ULA-9819	198.75	Shell	3285 ± 20	39 ± 63	2895 ± 105	−945 ± 105
	ULA-9820	259.50	Shell	4590 ± 15	39 ± 63	4565 ± 120	−2615 ± 120
COR20-02-18 GC	ULA-9654	80.25	Shell	1180 ± 15	39 ± 63	565 ± 70	1385 ± 70
	ULA-9682	204.50	Shell	3690 ± 20	39 ± 63	3395 ± 105	−1445 ± 105
	ULA-9620	213.25	Wood	3395 ± 15	–	3030 ± 80	−1135 ± 80
	ULA-9655	331.50	Shell	8485 ± 20	39 ± 63	8835 ± 125	−6885 ± 125
COR20-02-19 GC	ULA-925	14.00	Alga	Modern	–	−45 ± 5	1995 ± 5
	ULA-9646	201.50	Shell	2460 ± 15	39 ± 63	1885 ± 210	65 ± 210
COR20-02-20 GC	ULA-9650	40.00	Shell	790 ± 20	39 ± 63	205 ± 100	1745 ± 100
	ULA-9669	204.50	Shell	2255 ± 20	39 ± 63	1635 ± 100	315 ± 100
	ULA-9670	423.50	Shell	3915 ± 15	39 ± 63	3670 ± 110	−1720 ± 110
COR20-02-21 GC	ULA-9671	96.00	Shell	920 ± 15	39 ± 63	345 ± 85	1605 ± 85
	ULA-9672	178.50	Shell	2175 ± 15	39 ± 63	1545 ± 105	405 ± 105
COR20-02-50 GC	ULA-9784	46.50	Wood	Modern	–	−40 ± 5	1990 ± 5

Lawrence Estuary, though they are generally coarser in the Middle Estuary with 10% clay, 80% silt and 10% sand (e.g., COR20-02-50 GC). Likewise, the thickness of hemipelagites is between 10 and 20 cm in the Lower Estuary (e.g., COR20-02-50 GC) and higher than 50 cm in the Middle Estuary (e.g., COR20-02-04 GC).

On X-Ray images, light gray layers intersect the hemipelagic sedimentation. These layers correspond to RDL facies. Their physical properties, detailed below, contrast clearly with background sedimentation and their bases are mainly sharp, while their upper contacts are gradational. The internal structure and grain size distribution vary between RDLs, such that four groups can be distinguished: turbidites (T), debrites (D), hyperpycnites (H) and slump (S).

In the 15 cores, 43 turbidites (T) were identified (see supplementary data). Their thickness varies between ~3 and 73.5 cm with a mean value of 18.5 cm (Table 4). The bases are sharp and the grain size analyses reveal a normal grading typical of the Bouma-type turbidite (Bouma, 1962). Indeed, turbidites are characterized by a sandy base (fine to coarse sand) with sometimes gravels or rock fragments (<2 mm) as in turbidite T1 in core COR20-02-21 GC. The coarser material at the base of the turbidite layers is associated with high values of density and magnetic susceptibility, contrasting sharply with the overlying and underlying hemipelagic sediments. In core COR20-02-04 GC (Fig. 5), turbidite T1 presents a maximum density of 1.93 g cm^3 and a magnetic susceptibility of 744.10^{-5} SI, which both contrast with values of 1.45 g cm^3, and 144.10^{-5} SI in hemipelagic sediments. The coarse base of this turbidite layer likely comprises heavy minerals such as magnetite (e.g., Goldfinger et al., 2007; Jaegle, 2015) and is darker (L* = 37.5) compared to the under- and overlying background sediments (L* = 40.5), suggesting that this parameter could be used to discriminate the base of turbidites. Furthermore, the two chosen geochemical ratios in core COR20-02-04 GC are relatively constant in the hemipelagites (Zr/Rb = 1.22 and Ca/Fe = 0.34), but follow the grain size evolution of the turbidites with the highest values at the base (Zr/Rb = 14.75 and Ca/Fe = 0.43) gradually decreasing toward the top. These geochemical signatures, sensitive to grain size, can be used in addition to the previous parameters to accurately identify the base and top of turbidites.

Debrites (D) produced by debris flows constitute the second type of RDL identified in sediment cores. Only four debrites are identified in four cores. These deposits are more proximal to the source of submarine landslides than turbidites. The debrites include rock fragments up to ~10 cm in length, observable on XCT images (Fig. 6). As shown in D1 of core COR20-02-29 GC, these rock fragments vary in nature, size, angularity and orientation in a sandy-silty matrix composed of 75% sand, 20% silt and 5% clay (D_{50} ~150 μm). Thus, cores containing debrite layers are relatively short because the corer could not fully penetrate these deposits, unlike turbidites. Density and magnetic susceptibility are high with average values of respectively 1.95 g/cm^3 and 560.10^{-5} SI in core COR20-02-29 GC. In addition, contrary to turbidites, the debrites are massive and chaotic with no observable grading. The debrite in core COR07-03-11 PC (D1) (see supplementary data) is composed of a block of terrestrial organic material. Larger rock fragments are observed at the base of the debrite layer.

The RDLs characterized by reverse grading at the base followed by normal grading are interpreted as hyperpycnites (H) resulting from a hyperpycnal flow (Mulder et al., 2003; St-Onge et al., 2004). Hyperpycnites were observed in core COR20-02-26 GC (Fig. 5) recovered near the mouth of the Saguenay Fjord (~5 km). The

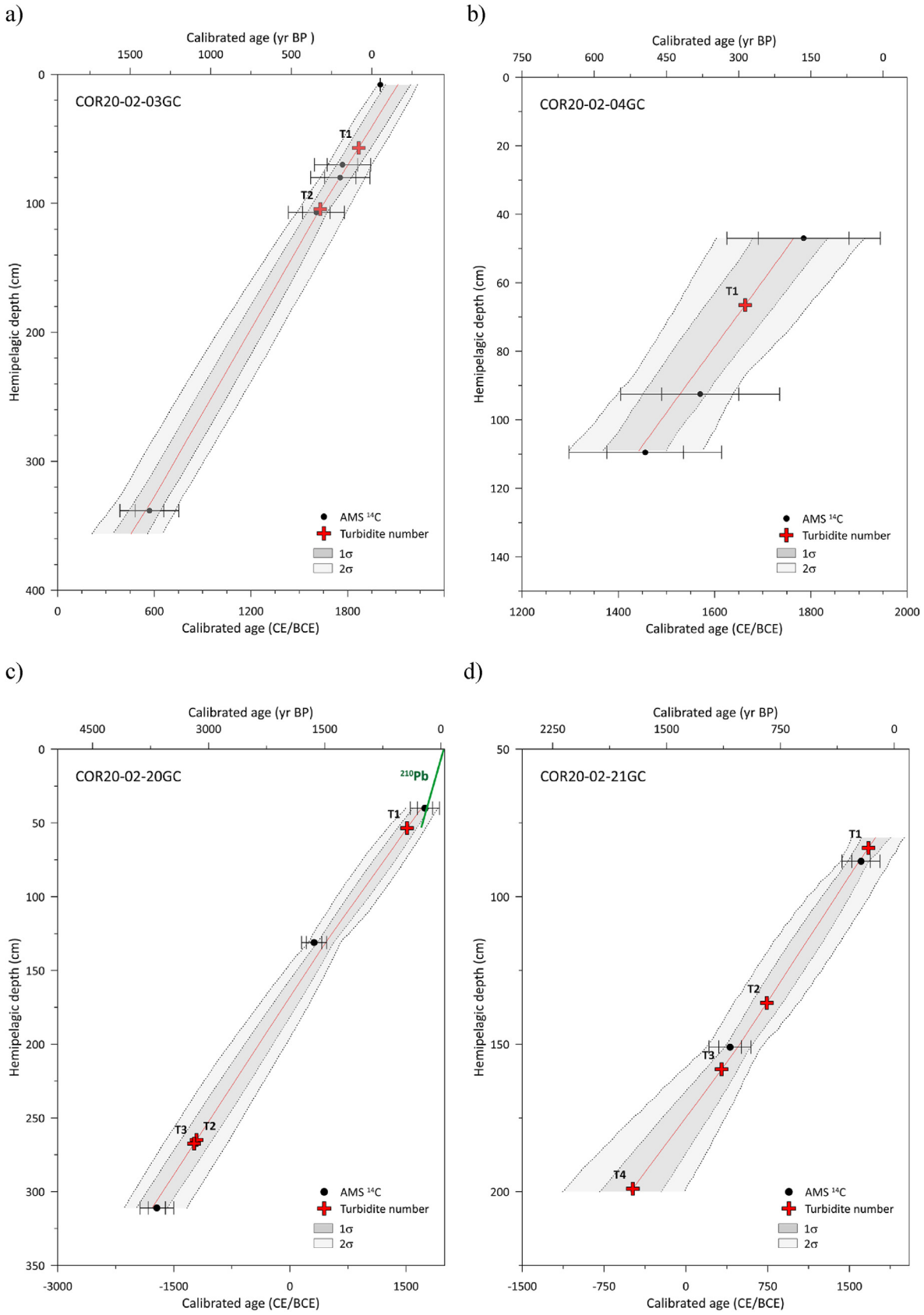

Fig. 7. Age models for cores COR20-02-03 GC a), COR20-02-04 GC b), COR20-02-20 GC c) and COR20-02-21 GC d). The hemipelagic depth, i.e., depth excluding RDLs, is plotted as a function of calibrated ages (BP and CE/BCE). The black circles correspond to the dated samples and the red crosses to the turbidites. The age probability of 2 σ and that of 1 σ, are respectively shown in light and medium gray tone. (For interpretation of the references to color in this figure legend, the reader is referred to the Web version of this article.)

Table 3
Sedimentation rates calculated and used in this study.

Box cores #	Date of sample (mm-dd-yyyy)	Sedimentation rate (cm.yr $^{-1}$)	Error ± 1 σ (cm.yr^{-1})
COR20-02-18BC-A	07-22-2020	0.32	0.045
COR20-02-20BC-B	07-23-2020	0.15	0.020
COR20-02-26BC-A	07-24-2020	0.42	0.040
COR20-02-28BC-B	07-24-2020	0.37	0.020

reverse grading at its base (256.5–226 cm) corresponds to the rising limb of the flood. Above 226 cm, the normal grading (226–190 cm) reflects the falling limb. Two hyperpycnites are also found in core COR20-02-50 GC (Fig. 6) sampled in the La Malbaie area.

A fourth type of RDL is characterized by the presence of a slump deposit (S) (Fig. 6). This deposit was found only at 100 cm in core COR20-02-50 GC. This is a 13.5-cm thick layer of silty-sand inducing peaks in density, magnetic susceptibility and Zr/Rb. The grains are not sorted and strong internal deformation is recognizable on the X-ray images. In summary, 43 of the RDLs are turbidites, four are debrites, three are hyperpycnites and one is a slump, highlighting the higher proportion of turbidites.

4.2. Age of the RDLs

The radiocarbon and ^{210}Pb results provided dating of 51 RDLs from 15 different cores (Table 4). The ages are between around 5035 cal yr BP and ~1991 CE. Only four age models are presented here (Fig. 7), the others are available in the supplementary data. In the next sections, the age of the RDLs are described for each area.

4.2.1. Baie-comeau

In the Baie-Comeau sector, turbidites T1, T2, T3, T4 and T5 in core COR20-02-13 GC were deposited respectively ~1145 CE, 520 CE, 4525 cal yr BP, 4905 cal yr BP and 4940 cal yr BP. In COR20-02-14 GC, four turbidites were deposited more recently around 1580 CE for the uppermost turbidite T1 and 1085 CE, 635 CE and 3270 cal yr BP for turbidites T2, T3 and T4.

4.2.2. Betsiamites-rimouski

Further west, in the Betsiamites area, the most recent turbidites (T1) in cores COR20-02-17 GC and COR20-02-18 GC are both dated ~ 1640–1680 CE while turbidite T2 in core COR20-02-17 GC is dated around 1560 CE. The age of the oldest turbidites is estimated at 5035 cal yr BP (T7) and 4830 cal yr BP (T6). Sedimentation rates calculated from the box core COR20-02-18BC-A provide respective ages of 1905 CE and 1805 CE for turbidites T1 and T2. In core COR07-03-13 PC recovered in the submarine landslide scar of the Betsiamites area, debrite D1 is estimated to be ~1650 CE based on dating of an intact block of terrestrial material. Turbidites T1 in cores COR20-02-04 GC and COR20-02-19 GC are dated to 1665 CE and 1690 CE respectively. Turbidite T2 in core COR20-02-19 GC is older with an age of 1115 CE. The ^{210}Pb-derived sedimentation rate of 0.32 cm.yr^{-1} in box core COR20-02-18BC-A yields more recent ages of 1880 CE and 1700 CE for T1 and T2 respectively. When considered for the nearby core COR07-03-11 PC, this sedimentation rate gives an age of 1865 CE for turbidite T1 and 1845 CE for T2. On the other side of the St. Lawrence Estuary, near of the city of Rimouski, turbidite T1 is dated at 1870 CE and T2 at 1630 CE.

4.2.3. Forestville

In core COR20-02-20 GC, collected in the Forestville area, turbidite T1 at a depth of 53.5 cm is dated at 1515 CE. Based on a ^{210}Pb-derived sedimentation rate of 0.15 cm.yr^{-1} calculated from the associated box core COR20-02-20BC-B, turbidite T1 dates back to 1665 CE. The older turbidites T2 and T3 are dated respectively to 3155 cal yr BP and 3190 cal yr BP. In core COR20-02-21 GC, recovered near a submarine landslide, turbidite T1 is observed at 83.5 cm depth and dated at 1675 CE. Turbidites T2, T3 and T4 in core COR20-02-21 GC have older ages of 745 CE, 325 CE and 2435 cal yr BP.

4.2.4. Saguenay

In the Saguenay area, the RDLs could not be dated by ^{14}C due to the absence of datable material. However, two sedimentation rates of 0.42 cm. yr^{-1} and 0.37 cm. yr^{-1} were calculated from the ^{210}Pb measurements in box cores COR20-02-26BC-A and COR20-02-28BC-B, respectively. The turbidite T1 found at 4 cm depth in core COR20-02-26 GC can thus be dated to 2010 CE, whereas turbidite T2 at 145 cm is dated at 1675 CE and the hyperpycnite H1 (158 cm) at 1645 CE. The debrite D1 identified in COR20-02-28GC-3 was dated at 1885 CE using the ^{210}Pb derived sedimentation rate of 0.37 cm. yr^{-1} in box core COR20-02–28BCE. Close to this coring site (~2.5 km), at the same water depth, core COR20-02-29 GC sampled the deposit linked to another submarine landslide. By using the sedimentation rate of box core COR20-02-28GC-3, the debrite D1 at 34 cm depth was dated at 1930 CE.

4.2.5. La Malbaie

In core COR20-02-50G from the Malbaie area, only one wood fragment could be sampled and dated at 1990 CE. As the hemipelagic sediments are close to the base of turbidite T1 from that core (~0.5 cm), we can consider an age of 1990 CE for T1. With seven RDLs preserved in a relatively short core (~2.28 m), core COR20-02-50 GC presents the highest frequency of RDLs of all the studied cores.

4.3. Correlation with seismic data

A sub-horizontal reflector with strong amplitude was identified at shallow depths (<2.0 m) on seismic profiles acquired across the different submarine landslide areas (Fig. 2). This reflector drapes the underlying sediments and is covered by a transparent acoustic facies (Figs. 2 and 3). According to the description and interpretation made by Cauchon-Voyer et al. (2008), the sedimentary deposits of the submarine landslide triggered by the 1663 CE earthquake were also characterized by the presence of a high amplitude reflector called R5 by these authors, underlying a transparent facies.

Near Rimouski, at the southern side of the Laurentian Channel, a reflector similar to R5 was identified in seismic profile RIM_1T (Fig. 3) at ~1.3 m depth below the deformed seafloor and shows an angular discordance with deeper, undisturbed reflectors. In the Betsiamites area, R5 type reflector was identified in seismic profile RIM_1A that crosses the lobe deposit of Betsiamites (Bernatchez, 2003) at a depth of ~0.75 m below the seafloor (Fig. 3). The deeper reflectors R1 to R4 and the seismic units U3 to U5 described by Cauchon-Voyer et al. (2008) are also visible and delimited. In seismic profiles BET_B_2T, R5 type reflector is found at a depth of ~1.8 mbsf (Fig. 3) while further to the south, it is identified at a depth of ~1.2 mbsf in the BET_D_2T profile (Fig. 3). In the Forestville area, the R5 type reflector is visible on both sides of the Laurentian

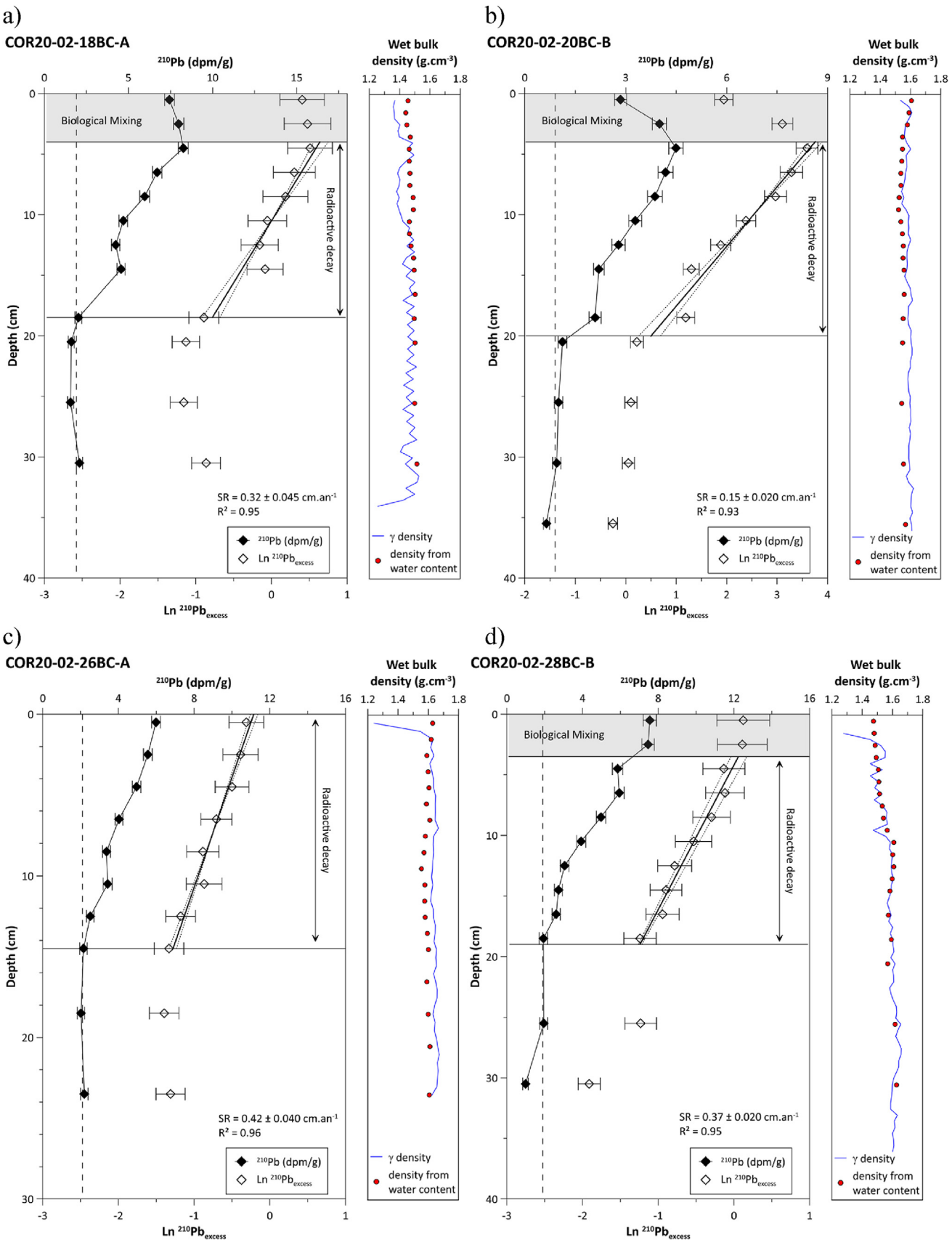

Fig. 8. Sedimentation rates (SR) calculated with the ^{210}Pb activity in cores COR20-02-18BC-A (SR = 0.32 cm.yr^{-1}, a), COR20-02-20BC-B (SR = 0.15 cm.yr^{-1}, b), COR20-02-26BC-A (SR = 0.42 cm.yr^{-1}, c) and COR20-02-28BC-B (SR = 0.37 cm. yr^{-1}, d). SR are calculated from the slope of Ln (^{210}Pb$_{excess}$) in the radioactive zone by excluding the biological mixing.

Table 4
Age^{14}C (CE/BCE) of turbidites, hyperpycnites and debrites identified in the 15 cores used in this study (see supplementary data for all age models and sedimentological analyses of all cores).

Layer	Total depth (cm)	Hemipelagic depth (cm)	Thickness (cm)	Type of deposit	Estimated ^{14}C age (yr BP), or (CE) when reported	Error ± 1 σ	Estimated age ^{210}Pb (CE)	Error ± 1 σ
Baie-Comeau								
COR20-02-13 GC								
RDL1	23	23	13	Turbidite	1145 CE	110		
RDL2	50.5	37.5	18.5	Turbidite	520 CE	260		
RDL3	181	149.5	11	Turbidite	4525	645		
RDL4	210.5	168	55.5	Turbidite	4905	640		
RDL5	268	170	33	Turbidite	4940	660		
COR20-02-14 GC								
RDL1	15	15	15	Turbidite	1580 CE	135		
RDL2	43	28	3	Turbidite	1085 CE	95		
RDL3	64	46	3	Turbidite	635 CE	315		
RDL4	153.5	132.5	8.5	Turbidite	3270	320		
Betsiamites								
COR20-02-17 GC								
RDL1	14	14	4.5	Turbidite	1680 CE	180		
RDL2	25.5	21	12.5	Turbidite	1560 CE	180		
RDL3	104	87	7	Turbidite	195 CE	220		
RDL4	124	100	11	Turbidite	2075	235		
RDL5	173	138	21.5	Turbidite	3020	175		
RDL6	241.5	185	15	Turbidite	4540	395		
RDL7	279	207.5	18	Turbidite	5035	430		
COR20-02-18 GC								
RDL1	37.5	37.5	13.5	Turbidite	1640 CE	100	1905	15
RDL2	82	68.5	10	Turbidite	1245 CE	135	1805	30
RDL3	167	143.5	22	Turbidite	3200	240		
RDL4	193	147.5	8	Turbidite	3335	225		
RDL5	236.5	183	38	Turbidite	4630	540		
RDL6	279	187.5	8.5	Turbidite	4830	590		
COR07-03-11 PC								
RDL1	50	50	62.5	Turbidite			1865	25
RDL2	118.5	56	126.5	Debrite			1845	25
COR07-03-13 PC								
RDL1	3	3	101.5	Debrite	1650 CE	5		
RDL2	357	354	25	Turbidite				
RDL3	386	358	11.5	Turbidite				
COR20-02-04 GC								
RDL1	66.5	66.5	11.5	Turbidite	1665 CE	70		
COR20-02-19 GC								
RDL1	44.5	44.5	4	Turbidite	1690 CE	90	1880	20
RDL2	107	103	10.5	Turbidite	1115 CE	140	1700	50
Rimouski								
COR20-02-03 GC								
RDL1	57	57	19.5	Turbidite	1870 CE	75		
RDL2	124	104.5	9	Turbidite	1630 CE	60		
Forestville								
COR20-02-20 GC								
RDL1	53.5	53.5	73.5	Turbidite	1515 CE	125	1665	35
RDL2	338.5	265	10.5	Turbidite	3155	140		
RDL3	351.5	267.5	28.5	Turbidite	3190	150		
COR20-02-21 GC								
RDL1	83.5	83.5	18	Turbidite	1675 CE	115		
RDL2	154	136	19.5	Turbidite	745 CE	140		
RDL3	196	158.5	10.5	Turbidite	325 CE	150		
RDL4	247	199	11	Turbidite	2435	275		
Saguenay								
COR20-02-26 GC								
RDL1	4	4	12	Turbidite			2010	5
RDL2	157	145	20	Turbidite			1675	30
RDL3	190	158	66.5	Hyperpycnite			1645	35
COR20-02-28GC-3								
RDL1	50	50	not fully cored	Debrite			1885	10
COR20-02-29 GC								
RDL1	34	34	not fully cored	Debrite			1930	5
La Malbaie								
COR20-02-50 GC								
RDL1	33.5	33.5	13	Turbidite	1990 CE	5		
RDL2	67	54	9	Turbidite				
RDL3	87.5	65.5	13.5	Slump				
RDL4	128.5	93	21.5	Hyperpycnite Turbidite				
RDL5	161	104	12.5	Hyperpycnite Turbidite				
RDL6	184	114.5	30					
RDL7	227	127.5	5					

Channel at a depth between ~1.0 mbsf and ~1.3 mbsf, in the seismic profiles FOR_A_1T and ESC_BCD_1T (Fig. 4). The R5 type reflector is again identified in the Saguenay area in seismic profile SAG_H_1T at about 2.0 mbsf depth (Fig. 4).

A correlation between sedimentological data and seismic profiles reveals that the R5 type reflector systematically corresponds to the base of RDLs. Thus, the RDLs correspond to strong sub-horizontal and parallel reflectors above and at the end of mass-transport deposits characterized by a chaotic and transparent seismic facies (Figs. 3 and 4). In the Betsiamites area, reflector R5 corresponds to the presence of turbidite T1 dated to 1665 CE in core COR20-02-04 GC. In COR20-02-19 GC, R5 corresponds to turbidite T2 estimated at 1700 CE based on the ^{210}Pb derived sedimentation rate. Turbidite T3 in core COR20-02-18 GC is also related to reflector R5 and is dated to 1570 CE based on the ^{210}Pb derived sedimentation rate. In the Rimouski area, turbidite T2 dated to 1630 CE is at the same depth as the R5 reflector. In Forestville, the turbidites T1 in core COR20-02-20 GC and T2 in core COR20-02-21 GC, are respectively dated around 1515-1665 CE and 1675 CE and located at a depth corresponding to that of reflector R5. Finally, this reflector is at the same depth as turbidites T2 or T3 in core COR20-02-26 GC collected at the mouth of the Saguenay River and dated between 1645 and 1675 CE. The similarity of these ages with the age interpreted by Cauchon-Voyer et al. (2008) confirms that the sub-horizontal reflectors described in the present study correspond to the seismic reflector R5.

A second reflector R6, shallower than R5 (<1 m) and characterized by a weaker amplitude is observed in the Betsiamites and Rimouski areas (Fig. 3). R6 correlates with the depth of turbidite T2 (~0.80 m) in COR20-02-18 GC, turbidite T1 (~0.50 m) in core COR20-02-19 GC, turbidite T1 or T2 (~0.50–1.20 m) in core COR07-03-11 PC and turbidite T1 (~0.60 m) in core COR20-02-03 GC. These three turbidites dated 1805 CE, 1690–1880 CE and 1870 CE, respectively.

5. Discussion

5.1. Relationship between submarine landslides and rapidly deposited layers (RDL)

The irregularity of deposits and the presence of coarse material and debris in submarine landslides makes coring difficult. During the SLIDE-2020 expedition, the coring sites were determined in order to overcome this limitation by targeting sub-horizontal reflectors in the distal part of submarine landslides where they are thin enough for their underlying and overlying sediments to be dated (e.g., Piper et al., 2019). The relationship between these reflectors and the mass-transport deposits is observed in the Betsiamites area (seismic profile BET_D_2T) and the Saguenay area (seismic profile SAG_H_1T) where the R5 reflector corresponding to RDLs is in the continuity with the sliding mass and above (Strachan, 2008). However, the fact that this geometry is not systematically identified, does not imply that this genetic link does not exist. Indeed, the coring revealed that the R5 reflector extending over the Lower Estuary corresponds to RDLs that may have been triggered by a submarine landslide or debris flow. The large number of turbidites observed in the cores recovered during the SLIDE2020 expedition validates their correspondence with sub-horizontal seismic reflectors distal to submarine landslides. Furthermore, it implies that the submarine landslides have progressively transformed into turbidity currents. The proximal turbidites have a higher proportion of coarse sediment (e.g., T2 in COR20-02-19 GC, d_{50} ~ 103 μm) than distal turbidites (e.g., T1 in COR20-02-04 GC, d_{50} ~ 28 μm) and the cores recovered from a site very close to mass transport deposits revealed debrites (e.g., COR20-02-29 GC) confirming that the RDLs are deposited by submarine landslides. The fragment of terrestrial soil in debrite D1 of core COR07-03-13 PC which may have been transported by the 1663 CE Colombier event along coast of the Betsiamites area (see Bernatchez, 2003) tends to support this relationship.

5.2. Chronology of the RDLs and triggering factors

The dated RDLs are assembled in Fig. 9. This figure reveals four distinct periods with at least twelve concomitant submarine landslides at the regional scale. The first period is between 1560 CE and 1710 CE with nine submarine landslides with a mean age of 1635 ± 75 CE spread over 140 km. RDLs deposited at this period correspond to reflector R5, observed regionally and dated to 1630 ± 65 CE (Fig. 9). The second period begins at 1800 CE and ends at 1900 CE. It includes six submarine landslides over a distance of 110 km and RDLs deposited in this period correlate with the seismic reflector R6 dated to 1830 ± 70 CE. The third period spans from 1910 CE to 1930 CE with two submarine landslide in the Betsiamites area and another 110 km away in the Saguenay. Finally, the fourth period extends from 1990 CE to 2010 CE with two submarine landslides 80 km apart.

The dating of RDLs presented in Table 4 includes ages beyond 2000 years, but they are not included in the synthesis in Fig. 9. Indeed, from ages older than 2000 years, the uncertainties become more important and it is difficult to establish with certainty that RDLs are synchronous. Moreover, it is not possible to establish a link between these deposits and historical seismicity.

During the four periods identified, four to five major historical earthquakes occurred in the St. Lawrence Estuary region (Lamontagne et al., 2018): 1663 ($M \leq 7$), 1860 ($M = 6.1$) or 1870 ($M = 6.6$), 1925 ($M = 6.2$) and 1988 ($M = 5.9$) (Table 5). The difference between the ^{14}C ages and ages calculated from sedimentation rates for the different RDLs may be related to the accuracy of the dating method and RDL thickness measurements. The most accurate cases correspond to turbidites T1 in cores COR20-02-04 GC and COR20-02-20 GC. Indeed, in core COR20-02-04 GC, turbidite T1 is already considered to be associated with the 1663 CE earthquake by Cauchon-Voyer et al. (2008) and has been dated at 1665 CE based on ^{14}C dating of the immediately underlying hemipelagic deposits. The ^{210}Pb dating of turbidite T1 in core COR20-02-20 GC yields an age of 1665 ± 35 CE, in agreement with the ^{14}C age considering the dating uncertainties (1515 CE ± 125 at 1σ and 1515 CE ± 245 at 2σ). The density profiles obtained with the MSCL and from water content measurements do not show a linear evolution with depth, but a rather stable density over the upper 2 m, suggesting that compaction can be neglected for the age calculations of the RDL with ^{210}Pb-derived sedimentation rates. The reliability of these dates supports the correlation between submarine landslides and historical seismicity but the close age of the 1860 and 1870 CE earthquakes does not lend to differentiate these events from our chronology owing to the age uncertainty of the dated RDLs.

Submarine landslides triggered by earthquakes have already been described in other regions of the world (e.g., Bryn *et al.*, 2005; Dan et al., 2009). Ground shaking during an earthquake constitutes a major factor for slope destabilization (Hampton et al., 1996) and its influence can exceed several hundreds of kilometers to trigger several independent failures (Goldfinger et al., 2012, 2017). The synchronicity between RDLs in a seismic region is increasingly used for the study of paleoseismicity during the Holocene (Goldfinger et al., 2007; Gracia et al., 2010; Ratzov et al., 2015; Howarth et al., 2021). Storms, river floods and rapid relative sea level rise can also trigger submarine landslides and turbidites at the regional scale (~100 km) (Talling, 2014). However, the RDLs in this study were not connected to river mouths. At the scale of the last 500

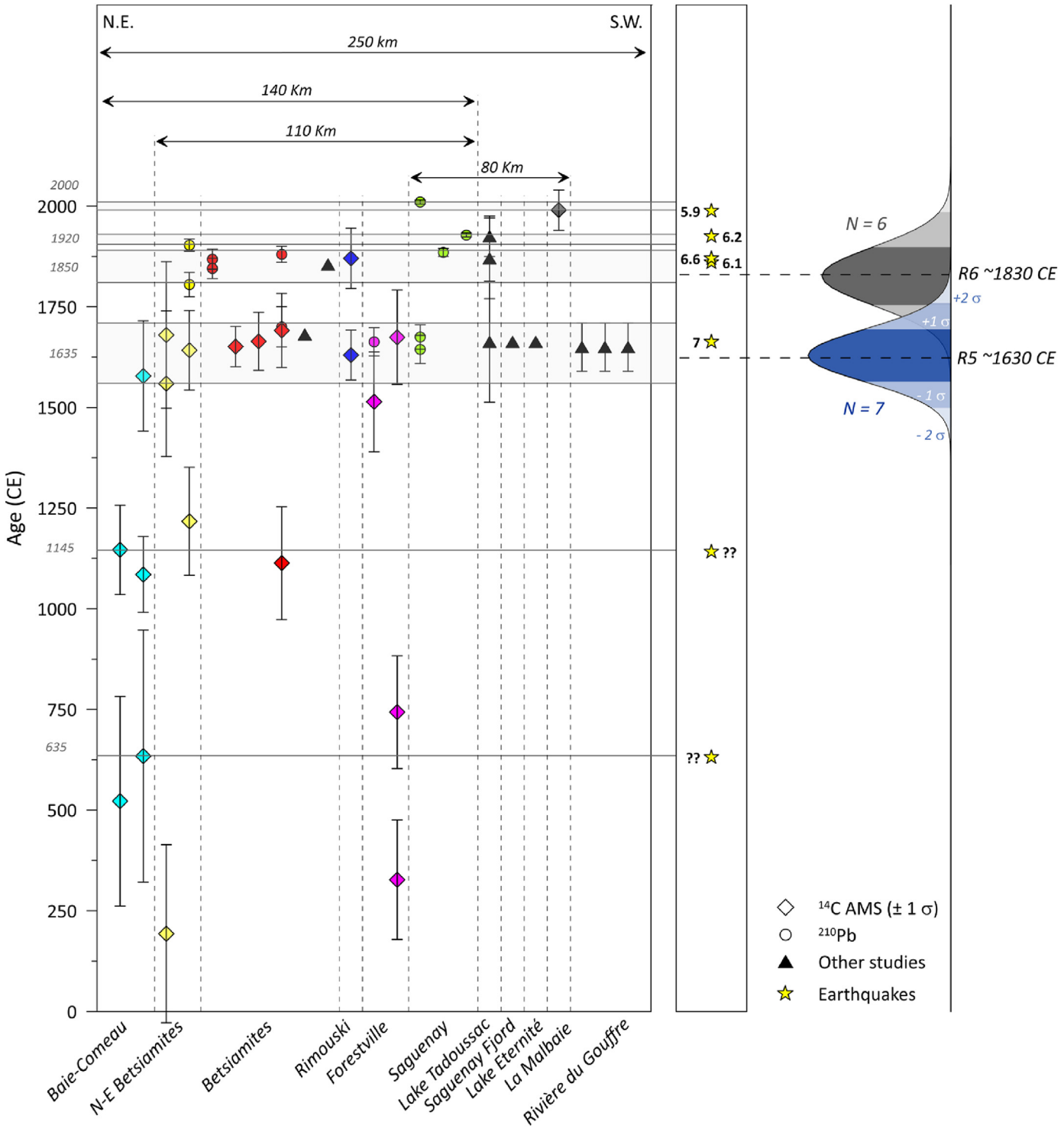

Fig. 9. Chronology of the RDLs (turbidites and debrites) dated by ^{14}C (colored diamonds) and ^{210}Pb (colored circles). The black triangles correspond to evidences provided by previous studies of aerial or submarine landslides in Québec (Doig, 1990; Filion *et al.*, 1991; St-Onge et al., 2004; Cauchon-Voyer et al., 2008; Locat et al., 2016). The gray intervals highlight periods of synchronous RDLs. The black arrows show the distance of synchronous submarine landslides for each period. The yellow stars indicate the timing of major historical earthquakes with their magnitude. To the right, the range of reflectors R5 (blue) and R6 (gray) considering a statistical error of ±1 σ and ±2 σ. (For interpretation of the references to color in this figure legend, the reader is referred to the Web version of this article.)

years, relative sea level variations are insignificant (Dionne, 2001; Shaw et al., 2002; Rémillard et al., 2017). Storms in eastern Canada are much weaker than tropical storms (e.g., Taiwan, New-Zealand) and the physiography of the estuary allows it to be relatively sheltered from oceanic swells (Bernatchez et al., 2012). Therefore, the synchronicity of submarine landslides that are reported here over a large area of a known seismic zone is a strong argument for relating their triggering to the regional seismicity of the CKBSL seismic zone.

The RDL 3 observed in core COR20-02-26 GC and dated around

Table 5
List of major historical earthquakes in the St. Lawrence Estuary (from Lamontagne et al., 2018).

Year	Lat (°N)	Long (°W)	Area	Magnitude	MMI	Magnitude information	Source
1663	47.60	−70.10	Charlevoix-Kamouraska	7.0	IX	Estimated	Gouin (2001)
1860	47.50	−70.10	Charlevoix-Kamouraska	6.1	VIII	Estimated	Gouin (2001)
1870	47.40	−70.50	Charlevoix-Kamouraska	6.6	IX-X	Estimated	(Gouin 2001)
1925	47.80	−69.80	Charlevoix-Kamouraska	6.2	VIII	Instrumented	Hodgson (1950); Bruneau and Lamontagne, 1994
1988	48.12	−71.18	Saguenay Region	5.9	VIII	Instrumented	North et al. (1989)

1645 CE in the Saguenay area is interpreted as a hyperpycnite. In the Saguenay Fjord, St-Onge et al. (2004) and Syvitski and Schafer (1996b) describe a similar deposit related to the 1663 CE earthquake. It was interpreted as a flood-induced hyperpycnal flow after the breach of a natural dam generated by an earthquake-triggered turbidite. Historical observations reported by the Jesuit mission and synthesized by Gouin (2001) support the generation of a hyperpycnal flow by the 1663 CE earthquake in the Saguenay area (e.g., Tadoussac) and throughout the estuary: *"Rivers were thoroughly polluted, the waters of some becoming yellow and of others red; and our great river St. Lawrence appeared all whitish as far as the region of Tadoussacq"*; *"displaced lands […] caused their gradual detrition by the water of the Rivers, which are still so thick and turbid as to change the color of the whole great St. Lawrence river."*

In the Middle Estuary, the tidal range and currents are stronger (Saucier and Chassé, 2000) as evidenced by the coarser sediments composing the hemipelagites observed in core COR20-02-50 GC. These forcings, particularly effective at low water depths could play a major role in preconditioning submarine landslides in the CKSZ, as currents can erode submarine slopes causing oversteepening (Hampton et al., 1996). These preconditioning factors combined with the high seismicity of the CKSZ (Lamontagne et al., 2018) could increase the submarine landslide hazard in the Middle Estuary, which in turn could explain the high frequency of RDL observed in core COR20-02-50 GC (four turbidites, two hyperpycnites and one slump). Moreover, the 1663 CE earthquake may have occurred in this region (Lamontagne et al., 2018).

5.3. Relative importance of the 1663 CE event

The 1663 CE earthquake was the strongest historical earthquake in Eastern Canada (Locat et al., 2003; Ebel, 2011; Lamontagne et al., 2018). This statement is confirmed by our study that allowed identifying at least 12 RDLs dated at ~1663 CE in 10 sediment cores distributed over a distance of 140 km, whereas only five RDLs dated at ~1860/1870 CE and two at ~1925 CE and ~1988 CE were observed over a less extensive area. The seismic survey revealed a strong shallow reflector present in almost all the studied area in the slopes and in the submarine landslide deposits. Intersecting cores analyzed and dated this reflector R5 (Figs. 3 and 4). Its approximate age is near to that of the 1663 CE earthquake. A second reflector has been identified (R6) and dated at about 1830−1860 CE, which is very close to the two other major historical earthquakes of 1860 and 1870 CE (Fig. 3). Shallower than R5, this seismic reflector is identified at fewer locations, confirming the relative importance of the 1663 CE earthquake compared to more recent events such as the 1860 and 1870 CE earthquakes.

In this study, it thus appears that the 1663 CE earthquake has triggered more submarine landslides over a larger area than more recent earthquakes (Fig. 9), attesting to the importance of this event at the scale of the last two millennia and corroborating historical observations reported by the first European settlers (Gouin, 2001; Ebel, 2011). Other studies in Québec (Doig, 1990; Filion et al., 1991; St-Onge et al., 2004; Cauchon-Voyer et al., 2008; Poncet et al., 2010a; 2010b; Locat et al., 2016) highlight the highest intensity of this major event. In comparison, more recent earthquakes (Table 5) appear to have had less impact than the 1663 CE earthquake. However, the relation between earthquake magnitude and the number of submarine landslides is not linear (e.g., Papadopoulos and Plessa, 2000). Some factors can interfere such as the sedimentary budget and predisposing factors (Hampton et al., 1996).

The compilation of submarine landslide ages leads to identify two older periods with synchronous ages of RDLs. The first at 1145 ± 145 CE with four synchronous deposits distributed over a distance of 40 km and the second at 645 ± 400 CE with three synchronous RDLs over a distance of 100 km. The first period has already been identified by Philibert , (2012) by the dating of RDL at ~ 1200 CE in Lake Jacques-Cartier (Fig. 1) and correlated with the seismicity of CKSZ. Moreover, Normandeau et al. (2013) found an earthquake-triggered submarine landslide deposit in Lake St-Joseph (Fig. 1) dated at ~1250 CE. Trottier et al. (2019) in Lake Maskinongé (CKSZ) also identified mass transport deposits about the same period at ~1180 CE through geomorphic and core analyses. Additionally, the major event identified and dated around 650 CE by Lajeunesse et al. (2017) in Lake Témiscouata near the Charlevoix area is likely synchronous with the RDLs dated at 645 ± 400 CE period in this study. The link between regional seismicity and the submarine landslides established in addition to these studies tends to suggest that two earthquakes could have triggered these older RDLs in the St. Lawrence Estuary.

6. Conclusions

The dating of 12 submarine landslides distributed over a distance of 220 km along the axis of the St. Lawrence Estuary allowed correlating them to the major historical earthquakes of 1663 CE, 1860 and/or 1870 CE and 1925 CE. The observation of older submarine landslide deposits suggests that two large earthquakes may have occurred around 645 CE and 1145 CE, in a period when historical data are not available. The criteria used to infer these relationships are:

(1) The careful location of the coring sites outside areas influenced by storms, sediment input (e.g., rivers) and active turbiditic channels;
(2) The ^{14}C and ^{210}Pb dating of turbidites and debrites revealing concomitant ages with the historical earthquakes;
(3) The synchronicity of submarine landslides and their associated turbidites described over a distance of ~220 km in a seismically active zone;

The results reported in this paper provide evidence that allow estimating the paleoseismicity of the last 2000 years in the St. Lawrence Estuary, which in turn improves the seismic hazard assessment in Eastern Canada. These results also allow demonstrating that the 1663 CE earthquake was the most important event of the last two millennia, although several submarine landslides observed in this study still remain to be dated. Investigating in detail these landslides would allow going even further back into the paleoseismological archives, refining the location of the epicenter

of the 1663 CE earthquake and assess landslide-related hazards. Additionally, characterizing of the mechanical behavior of sediments recovered in the St. Lawrence Estuary could help in evaluating the stability of slopes during an earthquake with specific attention on the stratified seismic unit 4, which seems susceptible to failure. Additional investigations are needed to characterize and understand the behavior and role of this unit during an earthquake, in particular its liquefaction potential.

Declaration of competing interest

The authors declare that they have no known competing financial interests or personal relationships that could have appeared to influence the work reported in this paper.

Acknowledgements

The authors wish to thank the captain and crew of the SLIDE2020 expedition on board the RV Coriolis II. They also thank Quentin Beauvais, Pascal Rioux and Sandrine Ouellet (ISMER) for their help in the laboratory, as well as Ray Burke for his contribution in the acquisition of geophysical data. The SLIDE2020 expedition was supported by ship time of the *Odyssée Saint-Laurent* program of the *Réseau Québec maritime* (RQM). G. St-Onge and P. Lajeunesse gratefully acknowledge the financial support of the Natural Sciences and Engineering Research Council of Canada (NSERC). Finally, the authors thank the two anonymous reviewers for their comments, which improved the quality of this paper.

Appendix A. Supplementary data

Supplementary data to this article can be found online at https://doi.org/10.1016/j.quascirev.2022.107640.

References

Adams, J., Basham, P., 1989. The seismicity and seismotectonics of Canada east of the Cordillera. Geosci. Can. 16, 3–16.
Anglin, F., 1984. Seismicity and faulting in the Charlevoix zone of the St. Lawrence valley. Bull. Seismol. Soc. Am. 74, 595–603.
Appleby, P.G., Oldfield, F., 1978. The calculation of lead-210 dates assuming a constant rate of supply of unsupported 210Pb to the sediment. Catena 5, 1–8.
Bernatchez, P., 2003. Évolution littorale holocène et actuelle des complexes deltaïques de Betsiamites et de Manicouagan-Outardes: synthèse, processus, causes et perspectives.
Bernatchez, P., Boucher-Brossard, G., Sigouin-Cantin, M., 2012. Contribution des archives à l'étude des événements météorologiques et géomorphologiques causant des dommages aux côtes du Québec maritime et analyse des tendances, des fréquences et des temps de retour des conditions météo-marines extrêmes. Rapport remis au ministère de la Sécurité publique du Québec. Chaire de recherche en géoscience côtière, Laboratoire de dynamique et de gestion intégrée des zones côtières, Université du Québec à Rimouski. Rimouski.
Blaauw, M., Christen, J.A., 2011. Flexible paleoclimate age-depth models using an autoregressive gamma process. Bayesian analysis 6, 457–474.
Bouma, A.H., 1962. Sedimentology of Some Flysch Deposits. Agraphic Approach to Facies Interpretation 168.
Bruneau, M., Lamontagne, M., 1994. Damage from 20th century earthquakes in eastern Canada and seismic vulnerability of unreinforced masonry buildings. Can. J. Civ. Eng. 21, 643–662.
Bryn, P., Berg, K., Forsberg, C.F., Solheim, A., Kvalstad, T.J., 2005. Explaining the storegga slide. Mar. Petrol. Geol. 22, 11–19.
Cauchon-Voyer, G., Locat, J., Leroueil, S., St-Onge, G., Demers, D., 2011. Large-scale subaerial and submarine Holocene and recent mass movements in the Betsiamites area, Quebec, Canada. Eng. Geol. 121, 28–45.
Cauchon-Voyer, G., Locat, J., St-Onge, G., 2008. Late-quaternary morpho-sedimentology and submarine mass movements of the Betsiamites area, lower St. Lawrence estuary, quebec, Canada. Mar. Geol. 251, 233–252.
Cauchon-Voyer, G., Turmel, D., Gagné, H., 2007. Rapport de mission COR0703, Estuaire du Saint-Laurent.
Croudace, I.W., Rindby, A., Rothwell, R.G., 2006. ITRAX: description and evaluation of a new multi-function X-ray core scanner. Geological Society, London, Special Publications 267, 51–63.
Dan, G., Sultan, N., Savoye, B., Deverchere, J., Yelles, K., 2009. Quantifying the role of sandy–silty sediments in generating slope failures during earthquakes: example from the Algerian margin. Int. J. Earth Sci. 98, 769–789.
Dionne, J.-C., 2001. Relative-sea-level changes in the St. Lawrence Estuary from deglaciation to present day. Deglacial history and relative sea-level changes, northern New England and adjacent Canada 351, 271–284.
Doig, R., 1990. 2300 yr history of seismicity from silting events, in Lake Tadoussac, Charlevoix, Quebec. Geology 18, 820–823.
Dubé, S., 1998. Analyse de l'écroulement rocheux du Mont Éboulé, (Québec).
Duchesne, M., Pinet, N., Bolduc, A., Bédard, K., Lavoie, D., 2007. Seismic Stratigraphy of the Lower St Lawrence River Estuary (Quebec) Quaternary Deposits and Seismic Signature of the Underlying Geological Domains. Geological Survey of Canada.
Duchesne, M.J., Pinet, N., Bédard, K., St-Onge, G., Lajeunesse, P., Campbell, D.C., Bolduc, A., 2010. Role of the bedrock topography in the Quaternary filling of a giant estuarine basin: the Lower St. Lawrence Estuary, Eastern Canada. Basin Res. 22, 933–951.
Ebel, J.E., 1996. The seventeenth century seismicity of northeastern North America. Seismol Res. Lett. 67, 51–68.
Ebel, J.E., 2011. A new analysis of the magnitude of the February 1663 earthquake at Charlevoix, Quebec. Bull. Seismol. Soc. Am. 101, 1024–1038.
Filion, L., Quinty, F., Bégin, C., 1991. A chronology of landslide activity in the valley of Rivière du Gouffre, Charlevoix, Quebec. Can. J. Earth Sci. 28, 250–256.
Goldfinger, C., Galer, S., Beeson, J., Hamilton, T., Black, B., Romsos, C., Patton, J., Nelson, C.H., Hausmann, R., Morey, A., 2017. The importance of site selection, sediment supply, and hydrodynamics: a case study of submarine paleoseismology on the northern Cascadia margin, Washington USA. Mar. Geol. 384, 4–46.
Goldfinger, C., Morey, A.E., Nelson, C.H., Gutiérrez-Pastor, J., Johnson, J.E., Karabanov, E., Chaytor, J., Eriksson, A., Party, S.S., 2007. Rupture lengths and temporal history of significant earthquakes on the offshore and north coast segments of the Northern San Andreas Fault based on turbidite stratigraphy. Earth Planet Sci. Lett. 254, 9–27.
Goldfinger, C., Nelson, C.H., Morey, A.E., Johnson, J.E., Patton, J.R., Karabanov, E.B., Gutierrez-Pastor, J., Eriksson, A.T., Gracia, E., Dunhill, G., 2012. Turbidite Event History—Methods and Implications for Holocene Paleoseismicity of the Cascadia Subduction Zone. US Geological Survey.
Gouin, P., 2001. Tremblements de terre historiques au Québec: de 1534 à mars 1925, identifiés et interprétés à partir des textes originaux contemporains. Guérin.
Gracia, E., Vizcaino, A., Escutia, C., Asioli, A., Rodes, A., Pallas, R., Garcia-Orellana, J., Lebreiro, S., Goldfinger, C., 2010. Holocene earthquake record offshore Portugal (SW Iberia): testing turbidite paleoseismology in a slow-convergence margin. Quat. Sci. Rev. 29, 1156–1172.
Hampton, M.A., Lee, H.J., Locat, J., 1996. Submarine landslides. Rev. Geophys. 34, 33–59.
Haworth, R.T., 1978. Interpretation of geophysical data in the northern Gulf of St. Lawrence and its relevance to lower Paleozoic geology. Geol. Soc. Am. Bull. 89, 1091–1110.
Heaton, T.J., Köhler, P., Butzin, M., Bard, E., Reimer, R.W., Austin, W.E., Ramsey, C.B., Grootes, P.M., Hughen, K.A., Kromer, B., 2020. Marine20—the marine radiocarbon age calibration curve (0–55,000 cal BP). Radiocarbon 62, 779–820.
Hodgson, E., 1928. The probable epicentre of the Saint lawrence earthquake of Feb. 5 1663. J. Roy. Astron. Soc. Can. 22, 325.
Hodgson, E.A., 1950. The St. Lawrence earthquake. Bull. Seismol. Soc. Am. 15 (2), 84–105.
Howarth, J.D., Orpin, A.R., Kaneko, Y., Strachan, L.J., Nodder, S.D., Mountjoy, J.J., Barnes, P.M., Bostock, H.C., Holden, C., Jones, K., 2021. Calibrating the marine turbidite palaeoseismometer using the 2016 Kaikōura earthquake. Nat. Geosci. 14, 161–167.
Jaegle, M., 2015. Nature et origine des sédiments de surface de l'estuaire du Saint-Laurent. Université du Québec à Rimouski.
Josenhans, H., Lehman, S., 1999. Late glacial stratigraphy and history of the Gulf of St. Lawrence, Canada. Can. J. Earth Sci. 36, 1327–1345.
King, L.H., MacLean, B., 1970. Origin of the outer part of the Laurentian Channel. Can. J. Earth Sci. 7, 1470–1484.
Lajeunesse, P., Sinkunas, B., Morissette, A., Normandeau, A., Joyal, G., St-Onge, G., Locat, J., 2017. Large-scale seismically-induced mass-movements in a former glacial lake basin: lake Témiscouata, northeastern Appalachians (eastern Canada). Mar. Geol. 384, 120–130.
Lamontagne, M., Beauchemin, M., Toutin, T., 2003. Earthquakes in the Charlevoix seismic zone, quebec. Int. J. Hydropower Dams 10, 98–99.
Lamontagne, M., Halchuk, S., Cassidy, J.F., Rogers, G.C., 2018. Significant Canadian Earthquakes 1600-2017. Geological Survey of Canada.
Lasalle, P., Chagnon, J.-Y., 1968. An ancient landslide along the Saguenay River, quebec. Can. J. Earth Sci. 5, 548–549.
Lebreiro, S.M., McCave, I.N., Weaver, P.P., 1997. Late Quaternary turbidite emplacement on the Horseshoe abyssal plain (Iberian margin). J. Sediment. Res. 67, 856–870.
Locat, J., 2011. La localisation et la magnitude du séisme du 5 février 1663 (Charlevoix) revues à l'aide des mouvements de terrain. Can. Geotech. J. 48, 1266–1286.
Locat, J., Martin, F., Levesque, C., Locat, P., Leroueil, S., Konrad, J.-M., Urgeles, R., Canals, M., Duchesne, M., 2003. Submarine Mass Movements in the Upper Saguenay Fjord,(Québec, Canada), Triggered by the 1663 Earthquake, Submarine Mass Movements and Their Consequences. Springer, pp. 509–519.
Locat, J., Turmel, D., Habersetzer, M., Trottier, A.-P., Lajeunesse, P., St-Onge, G., 2016. Earthquake Induced Landslides in Lake Eternité, Québec, Canada, Submarine

Mass Movements and Their Consequences. Springer, pp. 361–370.
Martin, F., Konrad, J.-M., Locat, J., Locat, P., Urgeles, R., Lee, H., 2001. Caracteristiques geotechniques et analyse du potentiel de liquefaction des sediments recents et post-glaciaires du fjord du saguenay. Quebec (Canada).
McNeely, R., Dyke, A.S., Southon, J.R., 2006. Canadian Marine Reservoir Ages Preliminary Data Assessment. Geological Survey of Canada.
Mulder, T., Syvitski, J.P., Migeon, S., Faugères, J.-C., Savoye, B., 2003. Hyperpycnal flows: initiation, behavior and related deposits. A review. Mar. Petrol. Geol. 20, 861–882. Marine.
Normandeau, A., Dietrich, P., Lajeunesse, P., St-Onge, G., Ghienne, J.-F., Duchesne, M.J., Francus, P., 2017. Timing and controls on the delivery of coarse sediment to deltas and submarine fans on a formerly glaciated coast and shelf. GSA Bulletin 129, 1424–1441.
Normandeau, A., Lajeunesse, P., Philibert, G., 2013. Late-Quaternary morphostratigraphy of Lake St-Joseph (southeastern Canadian Shield): evolution from a semi-enclosed glacimarine basin to a postglacial lake. Sediment. Geol. 295, 38–52.
Normandeau, A., Lajeunesse, P., St-Onge, G., 2015. Submarine canyons and channels in the Lower St. Lawrence Estuary (Eastern Canada): morphology, classification and recent sediment dynamics. Geomorphology 241, 1–18.
North, R.G., Wetmiller, R.J., Adams, J., Anglin, F.M., Hasegawa, H.S., Lamontagne, M., Berger, R.D., Seeber, L., Armbruster, J., 1989. Preliminary results from the November 25, 1988 Saguenay (quebec) earthquake. Seismol Res. Lett. 60, 89–93.
Obermeier, S.F., Martin, J., Frankel, A., Youd, T., Munson, P., Munson, C., Pond, E., 1992. Liquefaction Evidence for Strong Holocene Earthquake (S) in the Wabash Valley of Southern Indiana-Illinois, with a Preliminary Estimate of Magnitude. US Department of the Interior, US Geological Survey.
Ouellet, M., 1997. Lake Sediments and Holocene Seismic Hazard Assessment within the St. Lawrence Valley, Québec, vol. 109. Geological Society of America Bulletin, pp. 631–642.
Papadopoulos, G.A., Plessa, A., 2000. Magnitude–distance relations for earthquake-induced landslides in Greece. Eng. Geol. 58, 377–386.
Patton, J.R., Goldfinger, C., Morey, A.E., Ikehara, K., Romsos, C., Stoner, J., Djadjadihardja, Y., Ardhyastuti, S., Gaffar, E.Z., Vizcaino, A., 2015. A 6600 year earthquake history in the region of the 2004 Sumatra-Andaman subduction zone earthquake. Geosphere 11, 2067–2129.
Philibert, G., 2012. Évolution tardi-quaternaire du lac Jacques-Cartier, Réserve faunique des Laurentides. Québec.
Pinet, N., Brake, V., Campbell, C., Duchesne, M., 2011. Seafloor and shallow subsurface of the St. Lawrence river estuary. Geosci. Can. 38, 31–40.
Pinet, N., Brake, V., Campbell, C., Duchesne, M.J., 2015. Geomorphological characteristics and variability of Holocene mass-transport complexes, St. Lawrence river estuary, Canada. Geomorphology 228, 286–302.
Pinet, N., Duchesne, M., Lavoie, D., Bolduc, A., Long, B., 2008. Surface and subsurface signatures of gas seepage in the St. Lawrence Estuary (Canada): significance to hydrocarbon exploration. Mar. Petrol. Geol. 25, 271–288.
Pinet, N., Lamontagne, M., Duchesne, M.J., Brake, V.I., 2021. Hunting for Quaternary faults in eastern Canada: a critical appraisal of two potential candidates. Seismological Society of America 92, 1102–1111.
Piper, D.J., Tripsanas, E., Mosher, D.C., MacKillop, K., 2019. Paleoseismicity of the continental margin of eastern Canada: rare regional failures and associated turbidites in Orphan Basin. Geosphere 15, 85–107.
Poncet, R., Campbell, C., Dias, F., Locat, J., Mosher, D., 2010a. A Study of the Tsunami Effects of Two Landslides in the St. Lawrence Estuary, Submarine Mass Movements and Their Consequences. Springer, pp. 755–764.
Poncet, R., Campbell, C., Dias, F., Locat, J., Mosher, D., 2010b. A Study of the Tsunami Effects of Two Landslides in the St. Lawrence Estuary, Submarine Mass Movements and Their Consequences. Springer, pp. 755–764.
Riboulot, V., Cattaneo, A., Sultan, N., Garziglia, S., Ker, S., Imbert, P., Voisset, M., 2013. Sea-level change and free gas occurrence influencing a submarine landslide and pockmark formation and distribution in deepwater Nigeria. Earth Planet Sci. Lett. 375, 78–91.
Roy, D.W., DuBerger, R., 1983. Relations possibles entre la microseismicité récente et l'astroblème de Charlevoix. Can. J. Earth Sci. 20, 1613–1618.
Ratzov, G., et al., 2015. Holocene turbidites record earthquake supercycles at a slow-rate plate boundary. Geology 43 (4), 331–334.
Rémillard, A.M., St-Onge, G., Bernatchez, P., Hétu, B., Buylaert, J.-P., Murray, A.S., Lajeunesse, P., 2017. Relative sea-level changes and glacio-isostatic adjustment on the Magdalen Islands archipelago (Atlantic Canada) from MIS 5 to the late Holocene. Quat. Sci. Rev. 171, 216–233.
Saucier, F.J., Chassé, J., 2000. Tidal circulation and buoyancy effects in the St. Lawrence Estuary. Atmos.-Ocean 38, 505–556.
Seed, H.B., Idriss, I.M., 1967. Analysis of soil liquefaction: Niigata earthquake. J. Soil Mech. Found Div. 93, 83–108.
Shaw, J., Gareau, P., Courtney, R., 2002. Palaeogeography of Atlantic Canada 13–0 kyr. Quat. Sci. Rev. 21, 1861–1878.
Smith, W.T., 1962. Earthquakes of Eastern Canada and Adjacent Areas, 1534-1927. Department of Energy, Mines and Resources, Observatories Branch.
St-Onge, G., et al., 2012. Comparison of earthquake-triggered turbidites from the Saguenay (Eastern Canada) and Reloncavi (Chilean margin) Fjords: Implications for paleoseismicity and sedimentology. Sediment. Geol. 243, 89–107.
St-Onge, G., Lajeunesse, P., Duchesne, M.J., Gagne, H., 2008. Identification and dating of a key late Pleistocene stratigraphic unit in the St. Lawrence estuary and Gulf (eastern Canada). Quat. Sci. Rev. 27, 2390–2400.
St-Onge, G., Mulder, T., Francus, P., Long, B., 2007. Chapter two continuous physical properties of cored marine sediments. Developments in marine geology 1, 63–98.
St-Onge, G., Mulder, T., Piper, D.J., Hillaire-Marcel, C., Stoner, J.S., 2004. Earthquake and flood-induced turbidites in the Saguenay Fjord (Québec): a Holocene paleoseismicity record. Quat. Sci. Rev. 23, 283–294.
St-Onge, G., Stoner, J.S., Hillaire-Marcel, C., 2003. Holocene paleomagnetic records from the St. Lawrence Estuary, eastern Canada: centennial-to millennial-scale geomagnetic modulation of cosmogenic isotopes. Earth Planet Sci. Lett. 209, 113–130.
Strachan, L.J., 2008. Flow transformations in slumps: a case study from the Waitemata Basin, New Zealand. Sedimentology 55, 1311–1332.
Stuiver, M., Reimer, P.J., 1993. Extended 14C data base and revised CALIB 3.0 14C age calibration program. Radiocarbon 35, 215–230.
Syvitski, J., Praeg, D., 1989. Quaternary sedimentation in the St. Lawrence Estuary and adjoining areas, Eastern Canada: an overview based on high-resolution seismo-stratigraphy. Géogr. Phys. Quaternaire 43, 291–310.
Syvitski, J.P., Schafer, C.T., 1996a. Evidence for an earthquake-triggered basin collapse in Saguenay Fjord, Canada. Sediment. Geol. 104, 127–153.
Syvitski, J.P., Schafer, C.T., 1996b. Evidence for an earthquake-triggered basin collapse in Saguenay Fjord, Canada. Sediment. Geol. 104, 127–153.
Talling, P.J., 2014. On the triggers, resulting flow types and frequencies of subaqueous sediment density flows in different settings. Mar. Geol. 352, 155–182.
Trottier, A.-P., Lajeunesse, P., Normandeau, A., Gagnon-Poiré, A., 2019. Deglacial and postglacial paleoseismological archives in mass movement deposits of lakes of south-central Québec. Can. J. Earth Sci. 56, 60–76.
Tuttle, M.P., Atkinson, G.M., 2010. Localization of large earthquakes in the Charlevoix seismic zone, Quebec, Canada, during the past 10,000 years. Seismol Res. Lett. 81, 140–147.
Wu, P., 1998. Intraplate earthquakes and post-glacial rebound in eastern Canada and Northern Europe. Dynamics of the Ice Age Earth: A Modern Perspective 603–628.
Zhang, D., 2000. Flux de radio-isotopes à courte période dans les bassins marins marginaux de l'est canadien. Ph. D. thesis. Université du Québec à Montréal, Montréal, Québec.